The Astrophysical Journal, 673:1106–1122, 2008 February 1

CIRCUMSTELLAR DUST CREATED BY TERRESTRIAL PLANET FORMATION IN HD 113766

C. M. Lisse,[1] C. H. Chen,[2] M. C. Wyatt,[3] and A. Morlok[4]

Received 2007 April 9; accepted 2007 September 7

ABSTRACT

We present an analysis of the gas-poor circumstellar material in the HD 113766 binary system (F3/F5, 10–16 Myr), recently observed by the *Spitzer Space Telescope*. For our study we have used the IR mineralogical model derived from observations of the *Deep Impact* experiment. We find the dust dominated by warm, fine ($\sim$1 μm) particles, abundant in Mg-rich olivine, crystalline pyroxenes, amorphous silicates, Fe-rich sulfides, amorphous carbon, and colder water ice. The warm dust material mix is akin to an inner main-belt asteroid of S-type composition. The $\sim$440 K effective temperature of the warm dust implies that the bulk of the observed material is in a narrow belt $\sim$1.8 AU from the 4.4 $L_{\odot}$ central source, in the terrestrial planet–forming region and habitable zone of the system (equivalent to 0.9 AU in the solar system). The icy dust lies in two belts, located at 4–9 and 30–80 AU. The lower bound of warm dust mass in 0.1–20 μm, $dn/da \sim a^{-3.5}$ particles is very large, at least 3×10^{20} kg, equivalent to a 320 km radius asteroid of 2.5 g cm^{-3} density. Assuming 10 m particles are the largest present, the lower bound of warm dust mass is at least 0.5 $M_{\rm Mars}$. Neither primordial nor mature, the dust around HD 113766A originates from catastrophic disruption of terrestrial planet embryo(s) and subsequent grinding of the fragments or from collisions in a young, extremely dense asteroid belt undergoing planetary aggregation. The persistence of the strong IR excess over the last two decades argues for a mechanism to provide replenishment of the circumstellar material on yearly timescales.

Subject headings: infrared: stars — planetary systems: formation — planetary systems: protoplanetary disks — radiation mechanisms: thermal — techniques: spectroscopic

Online material: color figure

1. INTRODUCTION

We report here on an analysis of mid-IR observations of HD 113766, a young (10–16 Myr old), F3/F5 binary stellar system located at a distance of 130 pc from the Earth, with two component stars of nearly identical age characterized by early-F spectral types in the Sco-Cen association. Attention has been called to this system since its association with a detection in the *IRAS* Point Source Catalog (IRAS 13037−4545; Backman & Paresce 1993). More recent work by Meyer et al. (2001) and Chen et al. (2005, 2006) have confirmed that the system exhibits unobscured photospheres and a large IR excess ($L_{\rm IR}/L_* = 0.015$) but no detectable H I emission (Fig. 1). HD 113766A thus belongs to the small but growing class of post–T Tauri objects characterized by ages of 5–30 Myr with large quantities of excess mid-IR emission from hot dust, while lacking in significant gas. Similar objects have been identified in recent work: β Pic (Okamoto et al. 2004; Telesco et al. 2005), η Tel, and HD 172555, members of the β Pic moving group (Zuckerman & Song 2004); η Cha (Mamajek et al. 1999) and EF Cha (Rhee et al. 2007), members of the η Cha cluster; HD 3003, a member of the Tucana/Horologium moving group (Zuckerman et al. 2001); and eight objects in h and χ Per (Currie et al. 2007a, 2007b). It should be noted that the majority of post–T Tauri systems, e.g., the $\sim$10 Myr HD 99800B (Furlan et al. 2007) and the $\sim$30 Myr HD 12039 (Hines et al. 2006) of recent note, demonstrate IR excesses on the order of $L_{\rm IR}/L_* = 10^{-4}$, but from relatively cold dust with few strong mid-IR spectral features.

Of these young post–T Tauri objects dominated by warm dust, HD 113766 stands out as having the largest relative IR excess and strongest mid-IR spectral features (Rhee et al. 2007; Figs. 1 and 2). What makes HD 113766 so different? We find five possible physical scenarios to explain the strong excess emission: (1) the presence of significant residual primordial nebular material, (2) ongoing evaporation of material from a large swarm of primitive icy planetesimals (comets), (3) collisions of many bodies within a massive comet or asteroid (processed, differentiated planetesimals) belt, (4) a recent collision between two large comets or asteroids in a planetesimal belt, or (5) a recent collision between two protoplanets (e.g., the lunar formation event). (Note that for this work, a comet is defined as any $<$100 km, approximately half volatile ice, low-density and low-strength object with little to no processing of its constituent material vs. the material found in the protostellar nebula, while an asteroid is a $<$1000 km body with $<$20% volatile content and moderate to high density and strength which has undergone significant alteration due to thermal and/or collisional evolution. A prototerrestrial planet, derived from numerous asteroidal bodies, is a highly evolved and differentiated, high-density and high-strength body with $a > 1000$ km.)

The first scenario (1) is most likely ruled out from previous work. The HD 113766A disk is devoid of gas, as demonstrated for neutral hydrogen by Chen et al. (2006) (and by proxy for other gaseous species), and thus most primordial gas must have been removed. The extremely strong observed spectral features are direct evidence for the abundance of small ($\sim$1 μm) particulates, which have very short in-system lifetimes (on the order of years) due to the effects of radiation pressure ($\beta \sim 1$) and Poynting-Robertson (P-R) drag (Burns et al. 1979; Chen et al. 2006). This is a very different situation than is found in our stable, mature solar system debris disk (i.e., the interplanetary dust cloud), which is dominated

[1] Planetary Exploration Group, Space Department, Johns Hopkins University Applied Physics Laboratory, 11100 Johns Hopkins Road, Laurel, MD 20723; carey.lisse@jhuapl.edu.
[2] NOAO, 950 North Cherry Avenue, Tucson, AZ 85719; cchen@noao.edu.
[3] Institute of Astronomy, University of Cambridge, Madingley Road, Cambridge CB3 0HA, UK; wyatt@ast.cam.ac.uk.
[4] Department of Earth and Planetary Sciences, Faculty of Science, Kobe University, Nada, Kobe 657-8501, Japan; morlok70@kobe-u.ac.jp.

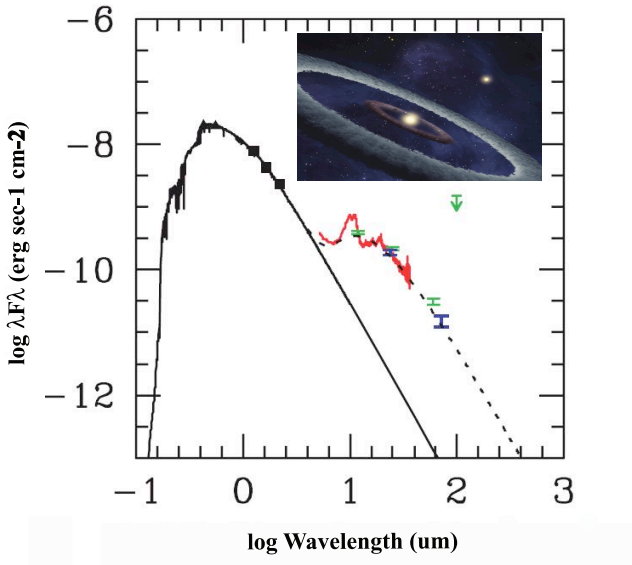

FIG. 1.—SED for HD 113766, after Chen et al. (2005, 2006). Tycho (*triangles*) and 2MASS (*squares*) photometric measurements are shown with filled black symbols; IRS spectra are shown in red; MIPS photometry, where available, is shown with blue error bars; and un-color-corrected *IRAS* photometry is shown with green error bars (12–60 μm) and an upper limit arrow (100 μm). The combined photospheric models are shown by the solid line. The dashed line is the best-fit constant emissivity model to the photometric points.

by large particles of sizes 20–2000 μm (Grogan et al. 2001) and dynamical lifetimes of 10^6–10^7 yr.

Because the HD 113766A phenomenon appears persistent from 1983 (*Infrared Astronomical Satellite* [*IRAS*]) until 2005 (*Spitzer*), we find that it must be persistent on timescales of decades, implying a continuous source of dust replenishment. The dynamical constraints, coupled with the estimated age of the system, suggest that the dust is being continuously replenished through sublimation of a large reservoir of planetesimals or collisions in such a reservoir. Thus, we must invoke scenarios like 2 and 3 above. A possible but less likely scenario is that the dusty material was created in a very recent impulsive fragmentation event involving an asteroidal, cometary, or protoplanetary body, with the produced dusty material slowly (on the order of decades) clearing out of the system (scenarios 4 and 5 above). In this case, any gas created by the fragmentation event must have been rapidly evolved, ionized, swept up by the local stellar wind, and removed from the system; otherwise, it would have been detected by *Spitzer*.

The occurrence rate of debris disks containing hot dust around Sun-like stars is very low, ~2% (Bryden et al. 2006; Chen et al. 2006). While recent work suggests that the hot dust of most mature Sun-like stars is transiently regenerated, as it is present in quantities far in excess of that expected to arise from sublimation of comets (Beichman et al. 2005) or slow collisional grinding of asteroids left over from the era of planet formation (Wyatt et al. 2007), HD 113766A is different, since its age is too young to consider it a mature debris disk. Rather, it must have emerged only recently (within the last 10 Myr) from its protoplanetary disk phase, and terrestrial planetesimal formation is most likely ongoing (terrestrial planets form on timescales of 10–100 Myr; Wetherill 1990 and references therein; Yin et al. 2002; Chambers 2004 and references therein).

During such an epoch large quantities of hot dust may be expected for a number of reasons. Terrestrial planets are thought to grow by accumulation of smaller objects, through the process of collisional accretion (Kenyon & Bromley 2004a, 2006). A few large bodies, or "oligarchs," of radii greater than a few hundred kilometers emerge from the swarm of initial kilometer-sized objects and dominate the system. Micron-sized dust is created during this aggregational phase, in a quantity on the order of a fraction of an Earth mass. The closer to the system primary the dust is created, the "drier" (or more volatile-poor) and warmer the dust will be. The resulting oligarchs stir up the remaining planetesimals into eccentric orbits, causing them to collide and fragment, clearing upward of 90% of the objects while producing a further collisional cascade and more circumstellar dust, in amounts rivaling the mass of Ceres or even the Moon (Table 3, discussed in § 4.3). The oligarchs become planets in this phase, objects like the Moon are created, and much of the collisionally produced dust created previously is swept up, while radiation pressure, P-R drag, and the stellar wind from the central source remove the rest (Kenyon & Bromley 2004b).

Enhanced warm circumstellar dust produced by the sum total of these terrestrial planet–forming processes, in amounts on the order of an oligarch ($M_{\rm Ceres}$ or larger), should be created and observable in the 10–100 Myr time frame. As the system relaxes from the era of planet formation over the next few gigayears, the dust density decreases by a few orders of magnitude, but eventually steady-state collisional grinding of small, leftover asteroidal bodies in planetesimal belts supports the bulk dust cloud at a low level, and stochastic asteroid fragmentation events in 1%–2% of stars produce rings of fresh dust analogous to the dust bands observed in the solar system zodiacal light (Bottke et al. 2005; Nesvorny et al. 2003, 2006) and the debris belt found around HD 69830 (Beichman et al. 2005; Lisse et al. 2007b).

The early studies of Schutz et al. (2005), using ESO TIMMI2 spectra, determined that the dusty material lay in a circumstellar belt around one of the HD 113766 stars and suggested that the 10 μm feature is dominated by crystalline silicate (forsterite) and large, amorphous silicates; SiO_2, which is correlated with the presence of forsterite in Herbig Ae/Be *ISO* spectra, was not detected. Chen et al. (2006) revisited this analysis and determined that HD 113766 possesses a large parent-body mass (0.1 $M_\oplus$, or 260 times the current mass in the solar system main asteroid belt) and a high single-blackbody grain temperature, $T_{\rm gr} = 330$ K, suggestive of debris at terrestrial planet temperatures. In a more detailed analysis, using a dust model of crystalline forsterite in addition to amorphous carbon, olivine, and pyroxene and a single-temperature blackbody continuum to fit the 5.5–35 μm Infrared Spectrograph (IRS) spectrum, they inferred a low crystalline silicate fraction of 4.1% for the dust. From their determination of the presence of a cooler blackbody continuum ($T_{\rm gr} = 200$ K) in addition to the hot silicate and carbon grains ($T_{\rm gr} = 600$ K), they suggested that this system possessed two planetesimal belts, analogous to our solar system's asteroid and Kuiper belts. The location of these hypothetical planetesimal belts was in the range $r_* = 0.5$–2.3 AU from the primary for the warm dust, comparable to the position of the asteroid belt in our own solar system, and at $r_* = 4$–5 AU for the cold dust.

No allowance was made in either of these spectral models, however, for effects due to particle size or composition. The recent findings on solar system primitive body mineralogy resulting from the *Deep Impact* and *Stardust* experiments allow us to greatly improve the models. *Spitzer* IRS observations of the *Deep Impact* experiment in 2005 July created a new paradigm for understanding the IR spectroscopy of primitive solar nebular material; the observed spectrum of fresh, interior ejected material was the most detailed ever observed. Further, the experiment provided a direct study of the thermal behavior of primitive nebular material in a known radiation field, allowing for empirical determination of the

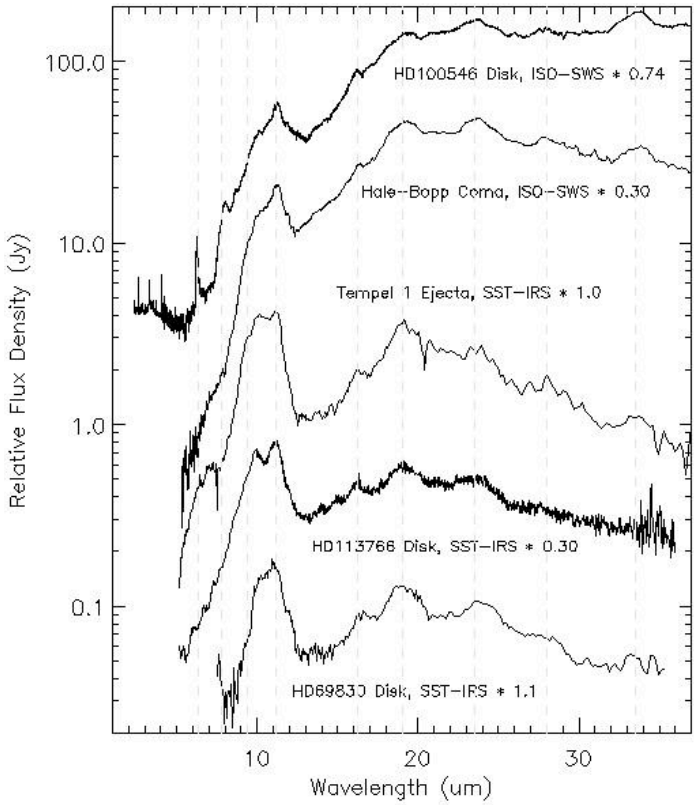

Fig. 2*a*

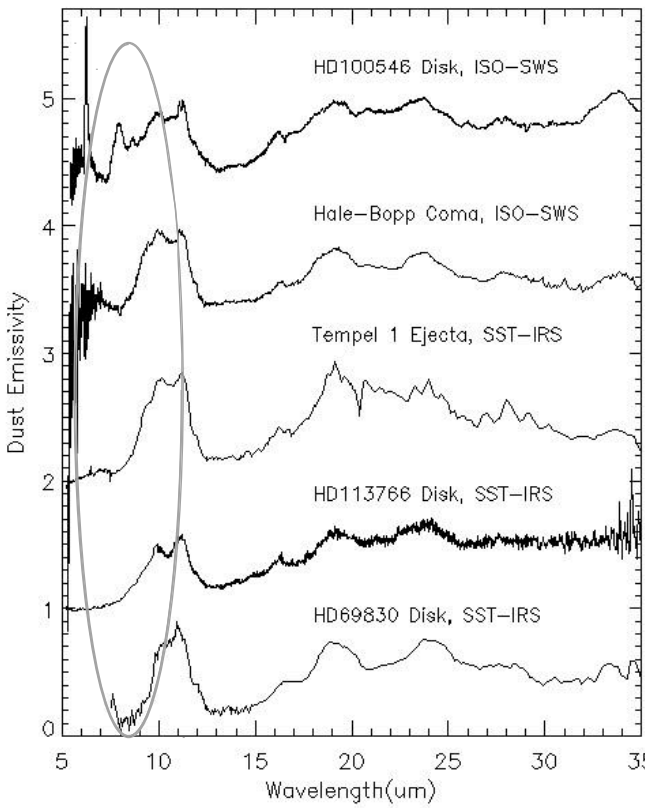

Fig. 2*b*

Fig. 2.—(*a*) Mid-IR spectra and (*b*) temperature-corrected dust emissivity spectra of the extremely young stellar object HD 100546 (after Malfait et al. 1998; Lisse et al. 2007a), the young terrestrial-planet-building system HD 113766, the mature solar system–like HD 69830 system (after Beichman et al. 2005; Lisse et al. 2007b), and the comets C/1995 O1 (Hale-Bopp) and T1 (after Lisse et al. 2006, 2007a), showing the gross similarities and major differences (*oval*) in the flux and particle emissivity for the sources. The uncertainty of each measurement can be estimated from the high-frequency variations in the data on wavelength scales of 0.05 μm. [*See the electronic edition of the Journal for a color version of this figure.*]

distance of the material in another system if the primary's luminosity is known. Decomposition of the *Deep Impact Spitzer* spectra implied the presence of seven classes of materials, including silicates, carbonates, phyllosilicates, water ice, amorphous carbon, PAHs, and metal sulfides (Lisse et al. 2006). The consistency of the results with the cometary material returned by the *Stardust* spacecraft from comet 81P/Wild 2, the in situ Halley flyby measurements, and the *Deep Impact* data return provide a fundamental cross-check for the spectral decomposition models. Further application of the model to the decomposition of the mid-IR spectra of comet C/1995 O1 (Hale-Bopp) and the circumstellar material found around the young stellar object (YSO) HD 100546 proved to be facile (Lisse et al. 2007a). In the next study, our group used the *Deep Impact* infrared mineralogical model to study the nature of the dust in the bright, dense debris disk found around the mature (2–10 Gyr old) K0 V star HD 69830 (Beichman et al. 2005). We were able to show that it was markedly different from any of the cometary systems we had studied: lacking in carbonaceous and ferrous materials but including small icy grains, and appearing to have composition much more like that of a disrupted, ~30 km radius P- or D-type asteroid from our solar system (Lisse et al. 2007b and references therein). The radiative temperature of the dust implied that the bulk of the observed material was at ~1.0 AU from the HD 69830 primary.

In this paper we utilize the *Spitzer* IRS observations of Chen et al. (2006) and our IR mineralogical model to further investigate the nature of the dust found around HD 113766A. We find that the circumstellar dust in the HD 113766A system is processed and differentiated and cannot be derived from cometary material; that it is much more rocky than the olivine-rich material found in the HD 69830 circumstellar belt, dominated by silicates (~75% crystalline), metal sulfides, and amorphous carbon, akin to the material found in S-type asteroids; that the composition of the refractory elements Si, Mg, Fe, Ca, and Al is close to solar and thus cannot be derived from the crust of a highly differentiated protoplanet; and that it is located in a belt at ~1.8 AU from the primary. Combining the low estimated age of the system, 10–16 Myr (based on its membership in the Lower Centaurus Crux part of the Sco-Cen stellar association), the similarity of the material to the most common asteroid type in the inner (terrestrial) portion of the solar system main asteroid belt, the very large amount of fine-dust present (0.5% of the lunar mass, or the mass of an S-type asteroid of radius 320 km), and the strong likelihood that this material is constantly being replenished, we find compelling evidence for ongoing terrestrial planet formation around HD 113766A. We find that the most likely source for the large amount of material detected by *Spitzer* and *IRAS* is the ongoing collisional grinding of an extremely dense young asteroid belt. It is also possible, but less likely, that the observed dust is due instead to the breakup and complete fragmentation of a large (>320 km radius) S-type body, on the order of a terrestrial planet embryo size and as large as the largest asteroid in our solar system. *Either of these possibilities are produced by formation processes associated with the building of terrestrial planets.*

2. OBSERVATIONS

The first indications of a large IR excess for the HD 113766 system were found in the *IRAS* sky survey (Backman & Paresce

1993; Fig. 1). Using mid-IR imaging photometry from the 6.5 m Magellan telescope, Meyer et al. (2001) found excess emission suggesting the presence of circumstellar dust around one of the two stars in the system, HD 113766A (Fig. 1), with a range of blackbody temperatures from approximately 290 to 440 K. (Note that only one of the stars, HD 113766A, shows a major IR excess, and throughout the text we use the terms "HD 113766A dust" or "HD 113766A excess" to refer to the circumstellar dust around HD 113766A and the term "HD 113766" to refer to the entirety of the binary system when the two component stars are considered as a unit or are unresolved.) The unresolved excess flux observed at 4.8, 11.7, and 18.0 μm appeared to originate from within 20, 50, and 80 AU, respectively, of HD 113766A. Including data obtained from the *Hipparcos* and Tycho photometric database (Fig. 1), Meyer et al. estimated the reddening and intrinsic stellar luminosity of the two binary components of HD 113766. Calculation of pre-main-sequence stellar evolution trajectories in the luminosity-temperature plane produced a stellar luminosity for HD 113766A and HD 113766B of $4.4 \pm 0.4\ L_{\odot}$ and an age for the stars of 10–20 Myr, consistent with their kinematic membership in the Lower Centaurus Crux subgroup of the Sco-Cen OB association. We adopt both of these values for the work presented here.

Chen et al. (2005) targeted 130 F-, G-, and K-type members of the young, nearby Sco-Cen association using *Spitzer* Multiband Imaging Photometer (MIPS) imaging photometric observations to study the transition from primordial to mature circumstellar disks and found HD 113766 to be one of 14 with appreciable excess 24 and 70 μm flux. In their follow-up study, which provided the data used in this work, Chen et al. (2006) obtained a *Spitzer* IRS 5–35 μm study of 59 main-sequence stars with previously reported *IRAS* 60 μm excesses (Sadakane & Nishida 1986; Sylvester et al. 1996; Walker & Wolstencroft 1988). HD 113766 was one of five conspicuous systems in their survey with large IR excess ($L_{\rm IR}/L_{*} = 0.015$) and extremely pronounced spectral features versus the spectral continuum.

For their IRS observations of HD 113766, Chen et al. (2006) utilized a combination of the Short-Low (5.2–14.0 μm, $\lambda/\Delta\lambda \sim 90$), Short-High (9.9–19.6 μm, $\lambda/\Delta\lambda \sim 600$), and Long-High (18.7–37.2 μm, $\lambda/\Delta\lambda \sim 600$) modules. A total of 1719 independent spectral points were obtained over the range 5.2–36 μm. In order to avoid time-consuming peak-up, the observatory was operated in IRS spectral-mapping mode, where a 2×3 raster (spatial $\times$ dispersion) centered on the star was performed (Watson et al. 2004). The reduction and analysis of the spectra were conducted with the *Spitzer* IRS instrument team's SMART program, version 15 (Higdon et al. 2004). Relative calibration of the spectral orders and fringing in the long-wavelength data were important issues that had to be dealt with in treating the data. We refer the reader to Chen et al. (2006) for more details of the IRS data reduction. The Chen et al. (2006) IRS spectrum for HD 113766 is overplotted on the stellar photometry in Figure 1.

The 5–35 μm HD 113766A disk excess flux studied in this work was calculated by removing the stellar binary photospheric contribution from the IRS spectrum of Chen et al. (2006). As HD 113766 is a binary system with a projected separation of 170 AU (1.3″), these objects were not separated by the *Spitzer* IRS and, thus, must be treated as a unit for purposes of photospheric modeling and removal. The photospheric contribution was modeled by assuming that the combined HD 113766A and HD 113766B spectrum is represented by an F3–F5 member of the Lower Centaurus Crux in Sco-Cen (de Zeeuw et al. 1999) with an estimated age of 16 Myr (Mamajek et al. 2002). Both component stars were assumed to have solar abundances, $\log g = 4.5$, and $E(B - V) = 0.01$ (determined using the Cardelli et al. [1989] extinction law). The stellar photospheric fluxes of the objects were then estimated by minimum χ^2 fitting of published unresolved photometry from the literature to model the combined Kurucz stellar atmospheres for the two sources, using only bandpasses with wavelengths shorter than 3 μm (Cutri et al. 2003). The photosphere-removed flux is presented and compared to other significant mid-IR dust spectra in Figure 2*a*.

3. MODELS

3.1. *The Deep Impact Tempel 1 Dust Model*

To understand the information derived from the HD 113766A excess IRS spectra, it is important to summarize the *Deep Impact* experiment and the Tempel 1 (T1) dust model. Details of the spectral analysis have been described in the literature in Lisse et al. (2006, 2007a). We only list the critical highlights here.

Spitzer IRS 5–35 μm spectra were taken immediately before and after the *Deep Impact* encounter, which occurred when T1 was 1.51 AU from the Sun on 2005 July 4. The material that was ejected from the nucleus from depths as large as 30 m was pristine and largely unaltered, due to the structural weakness of the material and the low escape velocity ($\sim$1 m s^{-1}) from the nucleus (A'Hearn et al. 2005). At the same time, it was de-aggregated from loosely held fractal particles into individual subfractal components (A'Hearn et al. 2005; Lisse et al. 2006; Sunshine et al. 2006). The observed material had cooled from effects due to the impact within minutes, and the separation of the ejecta from the ambient coma dust was cleanly made. The resulting highly structured spectrum of the ejecta showed over 16 distinct spectral features at flux levels of a few janskys (Lisse et al. 2006) that persisted for more than 20 hr after the impact. The preimpact spectrum showed almost no features and was well fit by a blackbody spectral model with a temperature near local thermodynamic equilibrium (LTE), indicative of the predominance of large, optical thick dust particles in the ambient coma.

The results of the *Deep Impact* experiment were observed by *Spitzer*, as well as 80 other observatories across the spectrum, allowing for multiple independent verifications of the behavior of a known quantity of astrophysical dust in a known radiation field. For example, Harker et al. (2005), Keller et al. (2005), Sugita et al. (2005), and Schleicher et al. (2006) have all published particle size distributions (PSDs) consistent with our findings (Lisse et al. 2006), and the *Deep Impact* near-IR spectrometer measured consistent effective temperatures for the ejecta (A'Hearn et al. 2005). The temperature and PSD of the ejected material did not have to be modeled or assumed; they were measured, as a result of one of the few astrophysical experiments performed to date.

The emission flux from a collection of dust is given by

$$F_{\lambda,\rm mod} = \frac{1}{\Delta^2} \sum_i \int_0^{\infty} B_{\lambda}[T_i(a, r_*)] Q_{{\rm abs},i}(a, \lambda) \pi a^2 \frac{dn_i(r_*)}{da}\, da,$$

where T is the particle temperature for a particle of radius a and composition i at distance r_* from the central star, Δ is the range from *Spitzer* to the dust, B_{λ} is the blackbody radiance at wavelength λ, $Q_{\rm abs}$ is the emission efficiency of the particle of composition i at wavelength λ, dn/da is the differential PSD of the emitted dust, and the sum is over all species of material and all sizes of particles for the dust. Our spectral analysis consists of calculating the emission flux for a model collection of dust and comparing the calculated flux to the observed flux. The emitted flux

depends on the composition (location of spectral features), particle size (feature-to-continuum contrast), and particle temperature (relative strength of short- vs. long-wavelength features), and we discuss each of these effects below.

Composition.—To determine the mineral composition, the observed IR emission is compared with the linear sum of laboratory thermal IR emission spectra. As-measured emission spectra of randomly oriented, 1 μm–sized powders were utilized to determine Q_{abs} in order to avoid the known inaccuracies and artifacts inherent in mathematical modeling (e.g., Mie theory) of strong emission features. The material spectra were selected by their reported presence in interplanetary dust particles, meteorites, in situ comet measurements, YSOs, and debris disks (Lisse et al. 2006). We originally tested for the presence of over 80 different species in the T1 ejecta, and we also checked for these species in other astrophysical dusty systems. The list of materials tested included multiple silicates in the olivine and pyroxene class (including forsterite, fayalite, clino- and ortho-enstatite, augite, anorthite, bronzite, diopside, and ferrosilite); phyllosilicates (such as saponite, serpentine, smectite, montmorillonite, and chlorite); sulfates (such as gypsum, ferrosulfate, and magnesium sulfate); oxides (including various aluminas, spinels, hibonite, magnetite, and hematite); Mg/Fe sulfides (including pyrrhotite, troilite, pyrite, and niningerite); carbonate minerals (including calcite, aragonite, dolomite, magnesite, and siderite); water ice, clean and with carbon dioxide, carbon monoxide, methane, and ammonia clathrates; carbon dioxide ice; graphitic and amorphous carbon; and the neutral and ionized PAH emission models of Draine & Li (2007).

The phase-space search excluded the vast majority of mineral species from the T1 ejecta. *From species comprising the best-fit model, Lisse et al.* (2006) *found convincing evidence for only the following as the majority species in the T1 ejecta*: crystalline silicates like forsterite, fayalite, ortho-enstatite, diopside, ferrosilite, and amorphous silicates with olivine- and pyroxene-like composition; phyllosilicates similar to notronite; metal sulfides like ningerite and pyrrhotite; carbonates like magnesite and siderite; water gas and ice; amorphous carbon (and potentially native Fe:Ni); and ionized PAHs. These seven classes of minerals (15 species in all) are the ones we have used in modeling other systems, including HD 113766.

Successfully applying our laboratory thermal emission spectra methodology to the spectra of three other solar system comets, three extrasolar YSOs, and two mature exo–debris disks has provided additional support for thermal IR emission signatures due to Ca/Fe/Mg-rich silicates, carbonates, phyllosilicates, water ice, amorphous carbon, ionized PAHs, and Fe/Mg sulfides, in varying proportions. This list of materials compares well by direct comparison to numerous in situ and sample return measurements (e.g., the Halley flybys and the *Stardust* sample return; see Lisse et al. [2007a] for a detailed list), providing a series of strong checks of its validity. A subset of this list was found to fit the HD 113766A spectrum well (Table 1; Fig. 3).

Of special note, our ability to detect water ice and gas has also been checked by comparing the results for the solar system comets versus their location with respect to the ice line. Comet SW3 (M. Sitko et al. 2008, in preparation) at 1 AU showed only water gas emission; comets Hale-Bopp (Malfait et al. 1998) at 2.8 AU and SW1 (Stansberry et al. 2004) at 5.2 AU showed only water ice; and comet T1 at 1.5 AU showed a mix, as the rapid excavation of material from the comet by the hypervelocity impact of the *Deep Impact* spacecraft ejected water ice from the nucleus in a nonequilibrium fashion, faster than the ice could sublimate (Sunshine et al. 2006).

Particle size effects.—Particles of 0.1–1000 μm are used in fitting the 5–35 μm data (although results to date have shown a sensitivity only to the 0.1–20 μm particle size range), with particle size effects on the emissivity assumed to vary as

$$1 - \text{emissivity}(a, \lambda) = [1 - \text{emissivity}(1\ \mu\text{m}, \lambda)]^{(a/1\ \mu\text{m})}.$$

The PSD is fit at logarthmic steps in radius, i.e., at 0.1, 0.2, 0.5, 1, 2, 5, . . . , 100, 200, and 500 μm. Particles of the smallest sizes have emission spectra with very sharp features and little continuum emission; particles of the largest sizes are optically thick and emit only continuum emission. Both the T1 ejecta spectrum and the HD 113766A spectrum show strong, sharp, high-contrast features indicative of the presence of small ($\sim$1 μm) grains. For the T1 ejecta, the PSD was found to be unusually narrow, consisting predominantly of 0.5–2.0 μm particles (Lisse et al. 2006). For the HD 113766A excess, a power-law spectrum of particle sizes, including both large and small grains, was found to be necessary to fit the data.

Particle temperature.—Dust particle temperature is determined at the same logarthmic steps in radius used to determine the PSD. Particle temperature is a function of both particle composition and size at a given astrocentric distance. The highest temperature for the smallest particle of each species is free to vary and is determined by the best fit to the data; the largest, optically thick particles (1000 μm) are set to the LTE temperature, and the temperatures of particles of in-between sizes are interpolated between these extremes by radiative energy balance. We model the unresolved dust excess around HD 113766A as a relatively localized dust torus and a disk as a superpositional sum of individual tori. It is often difficult to distinguish between the two cases. The material dominating the emission is the hottest and densest material, and for most disks, this is the unobscured material closest to the primary star in the observing beam, as the circumstellar material density and temperature both decrease with distance from the central star. On the other hand, if the circumstellar material is highly extended, the large range of temperatures for the dust serves to smear out any sharp spectral features. This is not the case observed for HD 113766.

The T1 ejecta were, by experimental design, all highly localized at 1.51 AU from the Sun. We use this fact to *empirically* determine the effective distance of the emitting material from HD 113766A. To do this, the best-fit model temperature for the smallest and hottest (0.1–1 μm) particles for each material from our analysis is compared to the temperatures found for the (0.5–2.0 μm) particles of the T1 ejecta (Lisse et al. 2006), using the relation

$$T_{\text{dust}} = T_{\text{T1 ejecta}}(L_*/L_\odot)^{1/4}(1.51\ \text{AU}/r_*)^{1/2},$$

where T_{dust} is the temperature of the dust around HD 113766A, $T_{\text{T1 ejecta}}$ is as given in Lisse et al. (2006; $\sim$340 K), L_* is the bolometric luminosity of HD 113766A, and r_* is the distance of the dust particle from HD 113766A.

Model summary.—Our method has limited input assumptions; uses physically plausible emission measures from randomly oriented powders, rather than artificially derived Mie values; and simultaneously minimizes the number of adjustable parameters. The free parameters of the model are the relative abundance of each mineral species, the temperature of the smallest particle of each mineral species, and the value of the PSD at each particle size (Table 1). The total number of free parameters in the model used to fit the IRS HD 113766A spectrum is as follows:

TABLE 1
COMPOSITION OF THE BEST-FIT MODEL TO THE *Spitzer* IRS HD 113766A SPECTRUM

Species	Weighted[a] Surface Area	Density (g cm^{-3})	Mol. Weight	N_{moles}[b] (Relative)	Model T_{max}[c] (K)	Model χ^2_ν (If Not Included)
Detections						
Olivines						
Amorphous olivine ($MgFeSiO_4$)	0.09	3.6	172	0.19	450	5.59
ForsteriteKoike (Mg_2SiO_4)	0.22	3.2	140	0.50	450	10.4
Forsterite38 (Mg_2SiO_4)[d]	0.14	3.2	140	0.32	450	6.31
Pyroxenes						
Amorphous pyroxene ($MgFeSi_2O_6$)	0.06	3.5	232	0.09	420	4.22
Ferrosilite ($Fe_2Si_2O_6$)	0.07	4.0	264	0.10	420	2.67
Diopside ($CaMgSi_2O_6$)	0.06	3.3	216	0.09	420	2.25
Ortho-Enstatite ($Mg_2Si_2O_6$)	0.04	3.2	200	0.06	420	1.63
Phyllosilicates						
Smectite notronite [$Na_{0.33}Fe_2(Si,Al)_4O_{10}(OH)_2 * 3H_2O$]	0.08	2.3	496	0.03	450	3.75
Metal sulfides						
Ningerite ($Mg_{10}Fe_{90}S$)[e]	0.26	4.5	84	1.4	450	12.5
Organics						
Amorphous carbon (C)	0.06	2.5	12	1.3	490	8.35
Water						
Water ice (H_2O)	0.15	1.0	18	0.83	200	5.56
Upper Limits and Nondetections						
Water						
Water gas (H_2O)	0.00	1.0	18	$\leq$0.00	200	1.03
Carbonates						
Magnesite ($MgCO_3$)	0.00	3.1	84	$\leq$0.00	450	1.03
Siderite ($FeCO_3$)	0.00	3.9	116	$\leq$0.00	450	1.03
PAHs						
PAH ($C_{10}H_{14}$)	0.02	1.0	$\langle 178 \rangle$	$\leq$0.011	N/A	1.03

NOTE.—Best-fit model $\chi^2_\nu = 1.03$ with power-law PSD $dn/da \sim a^{-3.48}$, 5–35 μm range of fit.
[a] Weight of the emissivity spectrum of each dust species required to match the HD 113766A emissivity spectrum.
[b] $N_{moles}(i) \sim$ density(i)/molecular weight(i) $\times$ normalized surface area(i). Errors are $\pm$10% (1 σ).
[c] All temperatures are $\pm$10 K (1 σ).
[d] Not found in cometary systems to date.
[e] A ningerite composition of $Mg_{25}Fe_{75}S$ may fit the data better.

15 relative abundances plus 15 hottest particle temperatures plus 1 power-law size index equals 31. Best fits are found by a direct search through (composition, temperature, size distribution) phase space.

It is important to note that our methodology has allowed us to get beyond the classical, well-known olivine–pyroxene–amorphous carbon composition to the second-order, less emissive species like water, sulfides, PAHs, phyllosilicates, and carbonates. On the other hand, there are limitations to our methods. There is no petrological or isotopic information, and the results returned are for bulk averages of the observed systems. For example, only very abundant species with strong emission features (>10% of the silicate emission peaks) will be detectable. In order to cover the large phase space of possible minerals present, we assume a linear mix of the extreme end states of each mineral system and a linear shift in the band positions and strengths between the end states. For example, we linearly adjust the balance of forsterite (Fo100, or $MgSi_2O_4$) and fayalite (Fa100, or $Fe_2Si_2O_4$) to fit the observed spectrum, allowing us to determine the total number of each atom present, but cannot distinguish between the presence of Fo50 ($FeMgSi_2O_4$) and a 50-50 mix of Fo100 + Fa100. The values in the compositional tables should be interpreted thusly. We also cannot distinguish easily between "glassy silicate of non-stoichiometric but near-olivine (or -pyroxene) composition" and "amorphous silicate of olivine (or pyroxene) composition," and so we assume the presence of stoichiometric glasses when modeling the glassy silicates. Emission by relatively cold material and optical depth effects can both serve to obscure material in the observed system, so that the amount of material reported in this work is a lower limit to the true system mass.

Despite these limitations, we are able to determine the overall amounts of the different major classes of dust-forming materials (olivines, pyroxenes, sulfides, water, etc.) and the bulk elemental abundances for the most abundant atoms in these materials (C, O, Si, Mg, Fe, S, and Ca). Applying our analysis, with a series of strong "ground truth" checks of its validity, is highly diagnostic for interpreting mid-IR spectra of distant dusty systems like YSOs, debris disks, and planetary nebulae.

3.2. *Application of the Tempel 1 Dust Model to the HD 113766A IR Excess Observations*

3.2.1. *Qualitative Spectral Comparison*

To zeroth order, marked similarities are found at the gross level between the spectral features for the HD 113766A IR excess and those seen in comets Hale-Bopp and T1, YSO HD 100546, and the mature asteroidal debris disk system HD 69830, motivating the in-depth spectral analysis presented here (Fig. 2*a*). The quality of the T1 spectrum, taken for an object at 0.75 AU distance under a controlled astrophysical experiment, is readily apparent. The HD 113766 excess spectrum, while somewhat more noisy, was obtained for the most distant object in the set—131 pc

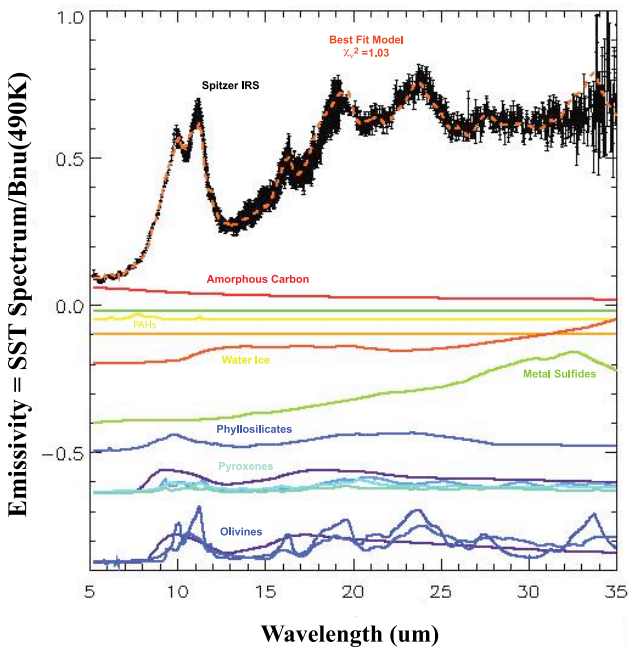

FIG. 3*a*

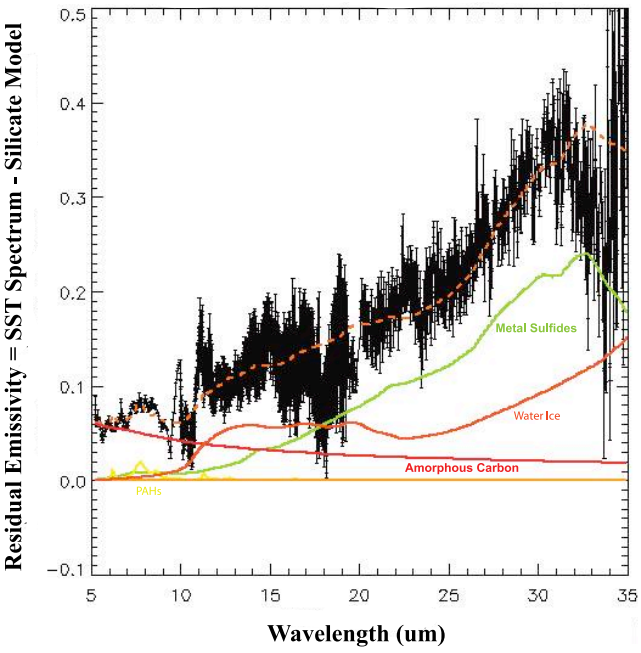

FIG. 3*b*

FIG. 3.—(*a*) *Spitzer* IRS emissivity spectrum of HD 113766, with best-fit spectral decomposition. The central source's photospheric contribution has been removed using a Kurucz model with a 6870 K photospheric temperature. Error bars are $\pm 2\ \sigma$. The amplitude of each colored curve denotes the relative amount of that species present in the best-fit model (Table 1). For species with no statistically detectable emission, the curve is a flat horizontal line. *Black line*: *Spitzer* excess spectrum, divided by a 490 K blackbody. *Orange dashed line*: Best-fit model spectrum. *Colored curves*: Emission spectra for the constituent species, scaled by the ratio $B_\lambda[T_{\rm dust}(a)_i]/B_\lambda(T_{\rm gr})$, with $T_{\rm gr} = 490$ K. *Purple*: Amorphous silicates of pyroxene or olivine composition. *Light blue*: Crystalline pyroxenes (ferrosilite, diopside, and ortho-enstatite). *Dark blue*: Crystalline olivine forsterites. *Red*: Amorphous carbon. *Dark orange*: Water ice. *Light orange*: Water gas. *Yellow*: PAHs. *Bright green*: Carbonates (siderite and magnesite). *Olive green*: Ferromagnesian sulfide $Fe_{0.9}Mg_{0.1}S$. (*b*) Residual emissivity of the circumstellar dust, after the emission due to the dominant silicates has been fit and removed. The remnant is dominated by emission from amorphous carbon, water ice, and metal sulfides. (Note that the $Fe_{0.9}Mg_{0.1}S$ emission spectrum used in our modeling could be improved to obtain a better fit; a ningerite with slightly increased Mg fraction, such as $Fe_{0.75}Mg_{0.25}S$, or a pyrrhotite is most likely indicated, but a good laboratory spectrum of these materials has yet to be measured.) While there are suggestions of possible water gas emission at 6 μm and carbon dioxide gas emission at 15 μm, neither of these features is statistically significant.

away—and is surprisingly bright, indicating that a large amount of emitting dust surface area is present in the observing beam.

Most of the obvious differences seen between the spectra of HD 100546 and Hale-Bopp and the other spectra in Figure 2*a* are due to temperature; the dust in T1, HD 113766, and HD 69830 is much warmer on average and, thus, has relatively more emission in the 5–10 μm region. Our analysis is done in emissivity space, as identification of emission lines due to different mineral species is easily and quickly done once the gross effects of temperature are removed (compare Figs. 2*a* and 2*b*). Conversion of the IR excess flux to an emissivity spectrum was performed by dividing the measured fluxes by a best-fit blackbody (with a value of $T_{\rm gr} = 490$ K found from χ^2 minimization testing, somewhat higher than the single-grain temperature of 330 K but comfortably between the 200 K cold dust and 600 K warm dust reported in Chen et al. [2006]; Fig. 2*b*).

Once the temperature effects are removed, many of the spectral features are seen at similar levels in all the emissivity spectra, including silicate emission features at 9.8, 11.2, 16.2, 19, 24, and 34 μm. These are the features that dominate the HD 113766A excess spectrum. Other major spectral features seen include the very strong PAH emission for HD 100546 at 6.2, 7.7, and 8.6 μm; water gas emission at $\sim$6 μm for HD 100546 and the comets; the carbonate peak for T1 at 6.5–7.5 μm; and the amorphous silicates at 8–9 μm in HD 100546, Hale-Bopp, and T1. The HD 100546 spectrum is dominated in the 5–8 μm region by spectral features due to carbon-rich species like PAHs and carbonates and water gas. The HD 113766A excess shows no evidence of emission from any of these species, suggesting the HD 113766A material has been processed to remove these volatile, nonrefractory materials (Fig. 2*b*, *oval*). On the other hand, unlike HD 113766A, the 2–10 Gyr old HD 69830 shows a strong lack of emission due to more easily processed pyroxene at 8–16 μm and a superabundance of the most refractory silicate, olivine. The HD 113766A silicaceous material is not as processed as the HD 69830 material.

3.2.2. *Mathematical Spectral Analysis*

More quantitatively, the resulting emissivity spectrum (Fig. 2*b*) was compared, using the methodology described in § 3.1, to linear combinations of laboratory emission spectra of 15 candidate mineral species (there are no obvious gas emission lines), selected for their reported presence in YSOs, solar system bodies, dusty disk systems, and interplanetary dust particles. We present here our best-fit compositional model (Fig. 3; Table 1) consisting of the fewest and simplest dust species possible that result in a consistent fit to the observational data. A set of components was tested exhaustively before the addition of a new species was allowed, and only species that reduced the χ_ν^2 below the 95% confidence limit (CL) were kept. It is important to emphasize that while the number of parameters (composition, temperature, and PSD) may seem large, there are, instead, very few detected species for the 1611 independent spectral points and 8 strong features obtained at high signal-to-noise ratio by the *Spitzer* IRS over the 5–35 μm range. It was, in fact, extremely difficult to fit the observed spectrum within the 95% CL of $\chi_\nu^2 = 1.03$. As discussed in § 3.1, when performing our spectral reduction, the detailed properties of the emitting dust (i.e., the particle composition, size distribution, and temperature) all have to be addressed. These

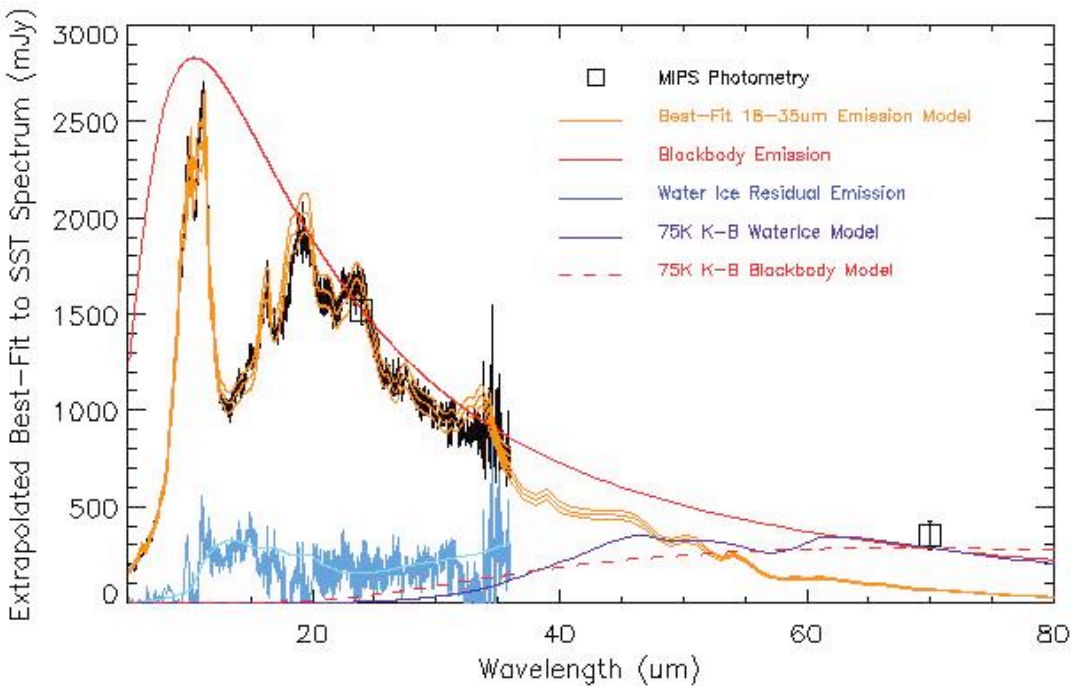

FIG. 4.—Comparison of the *Spitzer* MIPS 70 μm photometry and the best-fit model to the IRS 5–35 μm HD 113766 excess. The MIPS error bars are 2 σ. *Black line*: IRS data. *Orange line*: IRS emission model, extrapolated out to 80 μm. The model has been normalized at the nominal, +2 σ, and −2 σ MIPS 24 μm flux levels. The predicted flux of 67 ± 3 mJy from the best-fit model is less than 20% of the measured MIPS 70 μm flux of 350 ± 70 mJy. *Red solid line*: Warm blackbody model normalized to the 24 and 70 μm MIPS fluxes, demonstrating that a single system consisting of large, dark radiators cannot produce both the observed 5–35 and 70 μm emission. *Dark blue line*: Residual emission due to warm water ice, produced by subtracting all other model fluxes from the IRS data. *Light blue line*: Warm ice emission model flux. The purple curve shows the predicted flux from a reservoir of 75 K water ice particles with PSD $dn/da \sim a^{-3.5}$, required in addition to the warm dust dominating the 5–35 μm spectrum to produce the observed 70 μm MIPS flux. Emission from this population would be undetectable in the IRS bandpass. The dashed red curve shows the predicted flux from a collection of blackbody emitters at $T = 75$ K, which would also be undetectable in the IRS bandpass. It would be very hard to distinguish between these two models.

properties are thus all output products of the modeling and are available for interpretation, which we present in the next section. The possible range of each of the derived parameters was found by determining all models with $\chi^2_\nu < 1.03$. The resulting conservative ranges (2 σ) are ±20% for the abundance of each of the types of mineral species (Table 1), ±20 K for the maximum temperatures of the smallest dust, and ±0.2 for the slope of the PSDs.

4. DERIVED PROPERTIES OF THE DUST

4.1. *Composition and Atomic Abundance*

The derived compositional abundances from our best-fit dust model, with $\chi^2_\nu = 1.03$, are given in Table 1. As a test of the robustness of our best-fit model, the last column in Table 1 also gives the best-fitting χ^2_ν found after deleting a particular species from the compositional mix and refitting the data. Extensive searching of the possible compositional mixes, size distributions, and particle temperatures was conducted. The phase-space structure was found to be simple, with one deep minimum centered at the best-fit solution.

Overall, what we found is a very simple composition unlike the comets and comet-dominated YSO systems we have previously studied. The HD 113766A circumstellar dust spectrum can be reproduced using a simple mix of Mg-rich olivines (amorphous and crystalline), crystalline pyroxenes, and metal sulfides. The disk material appears to lack carbonaceous species like carbonates and PAHs and to have no Fe-rich olivines. The olivine crystalline fraction is 81%, similar to that found for the primitive comets and cometary exosystems (HD 100546, HD 163296), but the pyroxene crystalline fraction is also very high, ~74%, unlike cometary material, and the overall amount of amorphous pyroxene is highly depleted, suggesting that there has been some destruction of the less refractory amorphous pyroxene component in the HD 113766A material. These crystallinity values are sensible

TABLE 2
REFRACTORY DUST ATOMIC ABUNDANCES FOR OBJECTS OBSERVED BY *ISO* AND *Spitzer*

Object	H	C	O	Si[a]	Mg	Fe	S	Ca	Al
T1 ejecta	3.8E−4	0.052	0.46	1.0	0.82	0.79	0.61	0.84	1.0
Hale-Bopp coma	5.0E−05	0.13	0.23	1.0	1.1	0.97	0.63	0.45	1.4
HD 100546 (Be9 V)	1.1E−4	0.35	0.26	1.0	0.88	0.76	0.63	0.00	1.2
HD 69830	8.8E−06	0.088	0.18	1.0	1.1	0.43	0.00	0.93	0.0
HD 113766 (F3/F5)	3.0E−05	0.076	0.18	1.0	0.77	1.09	1.73	0.82	0.96

NOTE.—Abundance estimates have 2 σ errors of ±20%.
[a] All abundances are with respect to solar, with the Si abundance assumed to be 1.0 for normalization purposes.

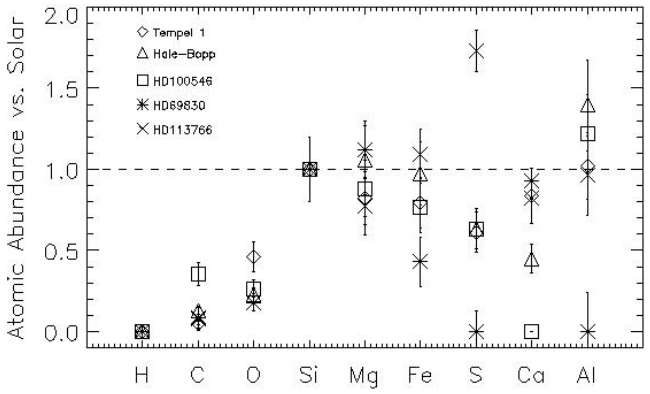

FIG. 5.—Atomic abundances for the refractory dust around HD 113766, compared to the published values for the comets T1 and Hale-Bopp, the comet-dominated YSO HD 100546, and the asteroidal debris disk system HD 69830 (Lisse et al. 2007a, 2007b). Abundances are given vs. solar, assuming Si = 1.0. Error bars for the relative measures are ±20% (2 σ). *Diamonds*, T1; *squares*, HD 100546; *triangles*, Hale-Bopp; *asterisks*, HD 69830. The nominal solar value is denoted by the dashed line. HD 113766 is normal vs. solar in the refractory species Si, Mg, Fe, Ca, and Al, similar to the cometary systems, and appears markedly abundant in S. Allowing for the large reservoir of unretained C, H, and O in volatile species, this dust appears to consist of a representative mix of the HD 113766 primordial nebular materials. Little atomic differentiation has occurred, except possibly for S.

given the extremely pronounced (vs. the continuum) silicate features, but are in sharp contrast to the value of 4.1% derived by Chen et al. (2006). The compositional makeup is almost equally divided, by mole, among the silicate, metal sulfide, and amorphous carbon species.

We also find a detection of warm water ice at 10–30 μm in our spectra (Fig. 4). The relative molar amount of water ice, ~0.17, is at the high end of the range found for the asteroidal material detected in the HD 69830 system (0.10–0.18). While thus plausible from a compositional point of view, it is not clear from a temperature analysis if the water ice is intrinsic to the hot refractory dust debris belt we find at 1.8 AU, nor if water ice would have lifetimes long enough to be found colocated with the warm dust belt. No significant emission due to water gas at 5–7 μm was found, consistent with the low neutral hydrogen/dust ratio found by Chen et al. (2006) for the system. (If water gas was present in large quantities, it would undergo UV photolysis to produce OH + H within 1 day in the HD 113766A radiation field.) The lack of water gas emission also argues against a large sublimation rate and the rapid creation of fresh, new water ice to replace the sublimation losses.

Our derived relative atomic abundances for the HD 113766A circumstellar material, H:C:O:Si:Mg:Fe:S:Ca:Al = 1.2:0.78:4.3:1.0:0.83:1.0:0.79:0.053:0.080 (assuming Si = 1.0), are very close to solar for all the refractory elements, Si, Mg, Fe, Ca, and Al, and are supersolar for S (Table 2). The estimated H, C, and O abundances are similar to those found for the comet-like systems (Fig. 5) and are reasonable for the amount of CHON material typically captured into a small primitive body of limited gravitational influence, with the remainder residing in the gas reservoir of the nebula and not the solids, in species such as H_2, H_2O, CO, CO_2, and CH_4 (Lisse et al. 2007a). (A similar level of C depletion is also found in CI chondrites and the Earth's crust; Ronov & Yaroshevsky 1969; Lodders 2003; Jura 2006.) The metallicity of the HD 113766 system has been estimated as close to solar, Fe/H = −0.02 (Nordstrom et al. 2004). As the abundances of the common refractory elements Si, Mg, Fe, S, and Al were found to be very close to solar for comet and comet-dominated YSO material (Lisse et al. 2007a; Fig. 5) and for CI chondrites and the Earth's crust, this strongly suggests that the HD 113766A circumstellar dust is similarly derived from a well-sampled mix of primordial nebular material, and little atomic differentiation has occurred.

4.2. *Temperature and Dust Location versus the Primary*

Our best models for the unresolved dust excess around HD 113766A are for localized dust tori. No extended runs of emitting material were required to fit the data, and as such we do not consider here the more complicated, higher degree of freedom disk models. The toroidal models are also motivated by the narrow dust structures found in many of the *Hubble Space Telescope* (*HST*) images of debris disks (Kalas et al. 2005, 2006), as well as the single-temperature distributions found for many of the objects studied by Beichman et al. (2006) and Chen et al. (2006). For example, the material detected around HD 69830 was determined by Lisse et al. (2007b) to reside in a torus at 1 ± 0.2 AU from the K0 V primary. (New observations using the Gemini 8 m telescope support this model, having confirmed that there is no obvious material from outside 2 AU [i.e., no extended disk] and probably demonstrating a marginal detection of the torus at 1 AU [C. A. Beichman et al. 2008, in preparation].) Further support for a narrow spatial distribution of the dust is found in the sharp, narrow spectral emission features (Fig. 3). If the warm dust were spread out over many AU, the dust grains would have a wide range of temperatures depending on particle size and heliocentric distance, and the ensemble sum of these different temperature grains would produce a broad, continuum-like emission, such as is found for the optically thin but highly extended disk of β Pic (Chen et al. 2007).

The "apparent" continuum dust temperature for the HD 113766A excess, $T_{gr} = 490$ K, is derived by directly matching a blackbody radiance curve to the observed run of flux with wavelength and is much higher than temperatures derived for a typical post–T Tauri system of similar age (e.g., $T_{gr} = 150$ K for the ~10 Myr HD 99800B [Furlan et al. 2007] and $T_{gr} = 110$ K for the ~30 Myr HD 12349 [Hines et al. 2006]) or the $T_{gr} = 250$ K found for the roughly coeval YSO Be9 V system HD 100546 (Lisse et al. 2007a). But it is near the $T_{gr} = 440$ K found for the warm asteroidal dust around the 2–10 Gyr old HD 69830 K0 V primary at a distance of 1 AU (Lisse et al. 2007b). Using our more detailed modeling methodology, we find that our best-fit temperature for the *smallest* dust particles of each material (0.1–1.0 μm), which superheat significantly above LTE, is 490 K for the amorphous carbon, ~450 K for the olivines, and ~420 K for the pyroxenes. These values are all comfortably close to each other, as expected for dust in relatively close physical proximity, and follow the rough $[Q_{abs}(\text{optical})/Q_{abs}(\text{IR})]^{0.25}$ law (Lisse et al. 1998), with the most optically absorbing material, amorphous carbon, being the warmest, and the most optically transparent pyroxenes somewhat cooler than the olivines (similar to the spectral modeling results found by Wooden et al. [1999] for comet Hale-Bopp). As for other systems, we note that the "apparent" continuum dust temperature, $T_{gr,}$ found by finding the best-fit single-blackbody match to the entire IRS spectrum, is close to the amorphous carbon hottest grain temperature, which dominates the continuum emission at short wavelengths (Fig. 3). As we have shown in § 4.1, however, amorphous carbon is only one of a number of species present in the system, and thus the single blackbody best for temperature should not be overinterpreted other than to be used as a coarse measure of the overall dust temperature and location. That is, given $T_{gr} = 490$ K, we can quickly ascertain that the average refractory dust particle temperature is between 400 and 500 K, and that given a 4.4 $L_\odot$ primary, the emitting dust must reside at a few AU from the central source.

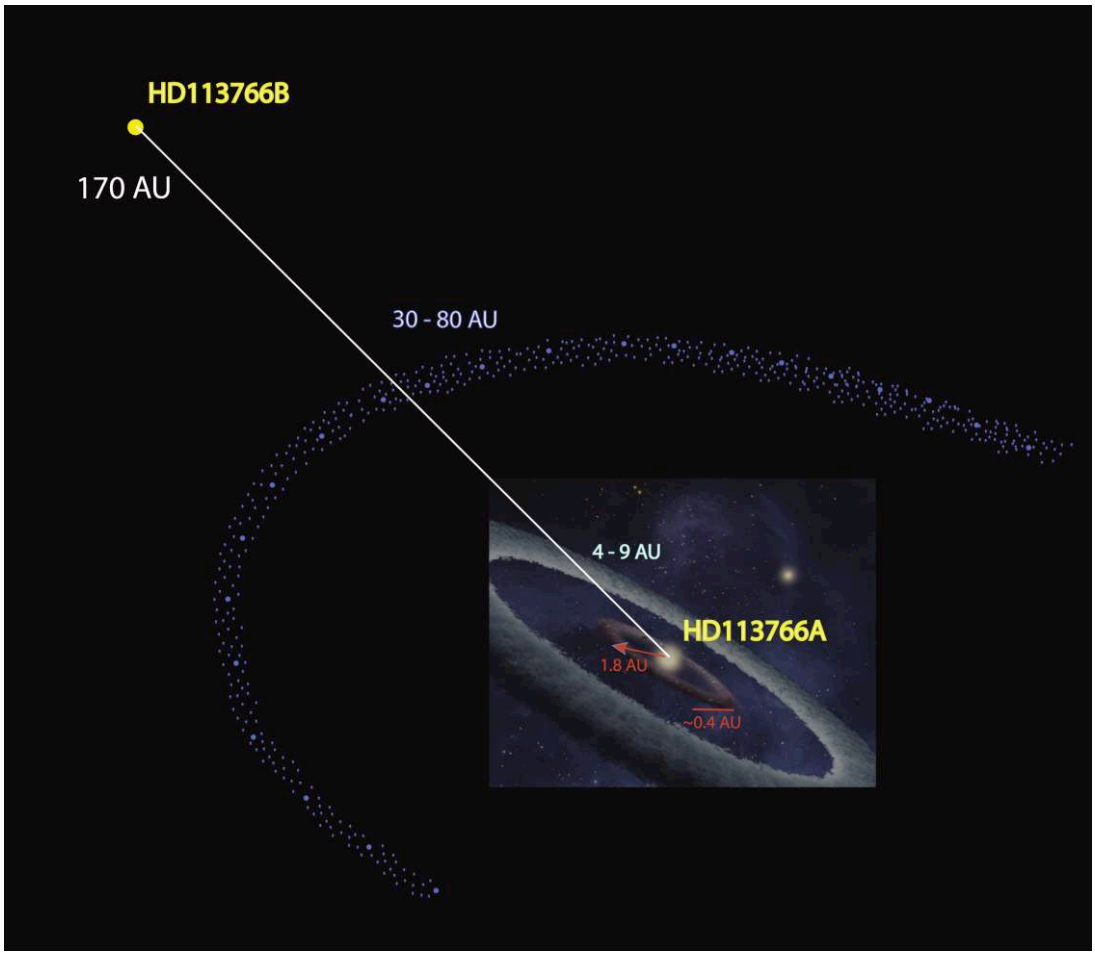

FIG. 6.—Schematic of the binary star system HD 113766. The location of the S asteroid–like dust causing the excess emission around HD 113766A found in this work, 1.8 ± 0.1 ($1\ \sigma$) AU (for $L_* = 4.4\ L_\odot$), is consistent with but more tightly constrained than the range found by Meyer et al. (2001; 0.35–5.8 AU). The nearby binary component, HD 113766B (distance not to scale), while potentially important for the dynamics of the system, is inconsequential for the energy balance of the inner-system dust causing the excess emission. The warm water-ice component detected can be anywhere within 9 AU of the HD 113766 stars, as determined by our analyses, including colocated within the dust ring, and another cold ice component is likely to be located at 30–80 AU.

Scaling empirically from the *Deep Impact* results (§ 3.1), we find for a 4.4 $L_\odot$ HD 113766A (Meyer et al. 2001; Chen et al. 2005) that we are observing a warm belt of dust located in the inner part of the system at 1.8 ± 0.10 ($1\ \sigma$) AU (Fig. 6). If this dust were in the solar system, undergoing irradiation at 1 $L_\odot$, and had the same effective temperature range (450 K for the smallest, warmest particles and 290 K for large, optically thick blackbody particles), it would lie at ~0.90 AU, very close to where the Earth lies. [Note that we have made these calculations ignoring the effects of the second star on the net insolation of the dust. Such an approach is physically valid, since the effect of the second star is negligible on dust at 1.8 AU from HD 113766A. If the two stars are of equal luminosity and HD 113766B is ~170 AU away, then the effect of the second star would be to increase the equilibrium temperature by a factor of $1 + 0.25(1.8/170)^2 = 1.00003$.]

This location of the warm HD 113766A dust in the heart of the terrestrial habitability zone of the system immediately suggests that we can expect similar nebular chemistry for the material that formed the Earth and the warm material detected in the HD 113766A disk, modulo the effects of the higher photospheric temperature (e.g., increased UV flux) and the potentially more massive protoplanetary disk mass in the HD 113766A system.

The apparent effective temperature of the smallest and warmest water ice particles in our best-fit model to the IRS data, ~200 K, is the temperature for ice at or just below sublimation equilibrium with vacuum; the temperature of pure water ice cannot vary above this value, as increases in input energy merely vaporize more water molecules. However, only very pure water ice will be unabsorptive and have long-term lifetimes at 200 K; as little as a few percent by mass of dark, absorbing material will cause a substantial increase of the radiative energy deposition into the ice, an increase in its temperature, a strong change in the dependence of temperature on particle size, and a drastic increase in its sublimation rate, and will reduce particle lifetimes to less than a few days (Lien 1990). If the water ice were intimately mixed together with the hot silicate/metal sulfide/amorphous carbon dust also detected by *Spitzer*, it would be actively subliming and require constant replenishment, as the lifetime for dirty water ice material at 1.8 AU from a $L_* = 4.4\ L_\odot$ primary is on the order of minutes to hours (Lien 1990). Since there is no indication of substantial water gas in the system, we conclude that the water ice detected is either extremely pure, colocated with the hot circumstellar dusty material at ~1.8 AU but poorly decoupled from the primary's radiation field, or, much more likely, "dirty"; i.e., it is mixed with as little as a few percent of dark, absorbing material but is at distances from the primary large enough so that sublimation losses are very small, lying outside the system's "ice line." The ice line for the smallest particles (0.1 μm) in our calculation lies at 9 AU (assuming $L_* = 4.4\ L_\odot$); for the largest (1000 μm), at 4 AU. The smallest particles will reach a temperature of 200 K at

TABLE 3
Derived Total Masses (in the Beam) for the Objects Observed by *ISO* and *Spitzer* and Selected Relevant Solar System Objects

Object	Observer Distance[a]	Mean Temp.[b] (K)	Equiv. Radius[c] (km)	19 μm Flux[d] (Jy)	Approximate Mass[e] (kg)
Earth	...	282	6380	...	6×10^{24}
Mars	1.5 AU	228	3400	...	6×10^{23}
Moon	0.0026 AU	282	1740	...	7×10^{22}
HD 100546 (Be9 V)	103.4 pc	250/135	$\geq$910	203	$\geq 1 \times 10^{22}$
HD 113766 (F3/F5)	130.9 pc	440	300–3000	1.85	3×10^{20}–3×10^{23}
Asteroid belt	0.1–5.0 AU	Variable	...	3×10^{21}	...
HD 69830	12.6 pc	340	30–60	0.11	3×10^{17}–2×10^{18}
Zody Cloud	0.1–4.0 AU	260	4×10^{16}	...	...
Asteroid	0.1–5.0 AU	Variable	1–500	...	10^{13}–10^{21}
Comet nucleus	0.1–10 AU	Variable	0.1–50	...	10^{12}–10^{15}
Hale-Bopp coma	3.0 AU	200	144	...	2×10^{9}
T1 ejecta	1.51 AU	340	3.8	1×10^{6}	...

[a] Distance from observer to object.
[b] Mean temperature of thermally emitting surface.
[c] Equivalent radius of solid body of 2.5 g cm^{-3}.
[d] System or disk averaged flux.
[e] Lower limits are conservative, assuming maximum particle size determined by *Spitzer* or *ISO* (20 μm), ignoring optical thickness effects. Upper limits assume a maximum particle size of 10 m radius.

any distance inside of 9 AU from HD 113766A but will evaporate quicker the closer they come to the star. Thus, we cannot be more definite about the location of the ice, due to the uncertainty brought into the physical picture by energy losses due to sublimation. We can say that we do not see significant emission due to water gas, so sublimation losses must be low, and it is most likely that the water ice lies in the 4–9 AU region, and the two sources of emission are simply confused along the line of sight in the large *Spitzer* IRS beam.

More support for the existence of unassociated icy dust reservoirs comes from studying the HD 113766A system at wavelengths longer than measured by the IRS. The *Spitzer* MIPS 70 μm channel is especially sensitive to cold (30–100 K) dust, and water ice has a strong emission feature at 65 μm. A MIPS photometric flux of 350 $\pm$ 35 (1 σ) mJy at 70 μm was reported for the system by Chen et al. (2006). Extrapolating our best-fit model spectrum out to longer wavelengths (Fig. 4), we find a predicted flux of, at most, 70 mJy at 70 μm. Something other than the hot dust at 1.8 AU and cold water ice at 4–9 AU must be providing the bulk of the observed 70 μm emission. A simple calculation shows that a second reservoir of very cold water ice ($T \leq 75$ K) or large blackbody particles ($T \leq 75$ K) can produce the remainder of the observed 70 μm flux, while adding negligibly to the 5–35 μm emission (Fig. 4). We cannot distinguish between these two models for the very cold dust from the given data, nor can we determine whether or not the dust is colder than 75 K. We do note that dust at 75 K would be at 30–65 AU from the HD 113766A primary, depending on particle size and composition, and thus resident in the system's equivalent of a Kuiper Belt; dust much farther out than 80 AU would be dynamically unstable because of HD 113776B, at 170 AU distance from HD 113766A (Fig. 6).

Thus, our model results are consistent with the conclusion that there is an icy dust population at a distance of $\sim$9 AU from HD 113766A (equivalent to icy material in the giant planet region of the solar system) and a second population of colder, icy Kuiper Belt dust farther from the primary at $r = 30$–80 AU ($T \leq 75$ K), contributing IR emission only at the longest wavelengths (Figs. 4 and 6). Abundant cold, icy dust is highly plausible; systems with 70 μm *Spitzer* excesses due to icy dust at distances $\sim$100 AU from the primary are relatively common (Bryden et al. 2006), and there are now a few examples of main-sequence systems as young as HD 113766 with copious amounts of distant, cold dust (e.g., TWA 7, Matthews et al. 2007; HD 99800B, Furlan et al. 2007; and HD 12349, Hines et al. 2006).

4.3. *Size Distribution and Total Mass*

The best-fit dust PSD found from our modeling, $dn/da \sim a^{-3.5\pm0.2}$ for particles with radius 0.1 μm $< a <$ 20 μm, argues for dust dominated by small particles in its emitting surface area and for a dust mass dominated by particles of the largest sizes. The predominance of small particle surface area is why we see the strong emission features; the dominant particles are optically thin, and the feature-to-continuum ratio is high. A similar PSD was found for Fomalhaut's disk (Wyatt & Dent 2002) and is the size distribution that is generally assumed for modeling debris disks (e.g., Augereau et al. 2001). A system in collisional equilibrium typically demonstrates a PSD $\sim a^{-3.5}$ (Dohnanyi 1969; Williams & Wetherill 1994; Durda & Dermott 1997). For "real" systems, a size distribution even steeper than $a^{-3.5}$ at small sizes is expected in a collisional cascade, both because of its truncation at the blow-out limit (Thebault et al. 2003) and because of the dependence of particle strength on size (O'Brien & Greenberg 2003). The fact that we see an $a^{-3.5}$ PSD in the system argues that the dust we are observing is relatively "fresh," at least on the radiation pressure timescales of years and P-R timescales of decades to centuries for 1 μm dust particles. By contrast, the mature solar system interplanetary dust cloud, close to equilibrium with the solar radiation field, has a very flat PSD devoid of small particles, $dn/da \sim a^{-1.4}$ (Grogan et al. 2001). Integrating the mass implied by the best-fit PSD, we find a dust mass of 3×10^{20} kg detected by the *Spitzer* 5–35 μm IRS spectrum (i.e., mass in particles of 0.1–20 μm in size that contribute appreciably to the observed emission and thus the χ^2_n value of the model fit). The dust mass of 3×10^{20} kg is $\sim$0.5% of the lunar mass, or the mass of an S-type asteroid of radius $\geq$320 km, 10^2 times the dust mass that is found in the mature dust clouds surrounding HD 69830 and 10^4 times the dust mass that is found around the Sun (Table 3). We quote this number here as the amount of mass definitively detected by the *Spitzer* observations.

However, the majority of the mass is in the largest, optically thick particles if they are present ($M_{\rm total} \sim a^{0.51}$), and there is no reason to believe that the maximum particle size is $\sim$20 μm.

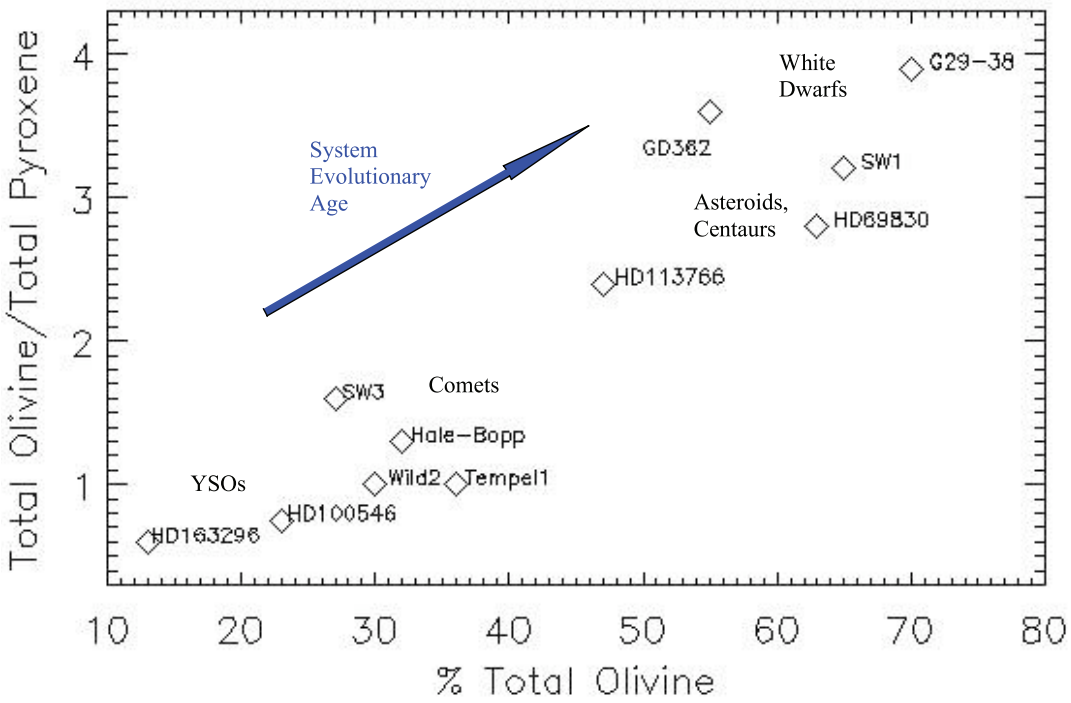

FIG. 7.—Silicate mineralogy for HD 113766 vs. that found in four comet systems (SW3, M. Sitko 2007, private communication; Hale-Bopp, Lisse et al. 2007a; Wild 2, Zolensky et al. 2007; and T1, Lisse et al. 2006), the primitive YSO disk systems HD 100546 (Lisse et al. 2007a) and HD 163296, the mature asteroidal debris belt system HD 69830 (dominated by P/D-type outer asteroid dust; Lisse et al. 2007b), the Centaur SW1 (Stansberry et al. 2004), and the ancient debris disk of white dwarfs G29-38 (Reach et al. 2005) and GD 362 (Jura 2006). The general trend observed is that the relative pyroxene content is high for the most primitive material (i.e., YSOs) and low for the most processed (i.e., white dwarfs). HD 113766 plots to the primitive side of the asteroidal region.

While the *Spitzer* IRS measurements are not very sensitive to larger grains, the SED compiled by Chen et al. (2006) for HD 113766 includes a high signal-to-noise ratio photometric detection of the system at 70 μm (*Spitzer*) and a 3 σ upper limit at 100 μm (*IRAS*). Direct interpolation of our best-fit compositional model, using a $dn/da \sim a^{-3.5}$ PSD for particles of sizes from 0.1 to 100 μm (here we explicitly include up to 100 μm grains in our modeling, as the longer wavelengths being considered have appreciable contributions from larger grain sizes than 20 μm), can only account for at most 20% of the 70 and 100 μm emission, and there must be another source of IR flux in the system, such as cold dust of $T \leq 75$ K (Fig. 4). Because it is also possible that all the 70 and 100 μm flux arises from the cold dust, we cannot state conclusively that the warm dust has particles larger than 20 μm. Future submillimeter and radio measurements, sensitive to larger particles due to their longer wavelengths, will be required to do so.

If, following Beichman et al. (2005), we instead estimate the amount of warm dust mass by assuming a PSD of constant slope up to a maximum size of 10 m in the HD 113766A circumstellar disk, we find a total mass of at least 3.4×10^{23} kg, or 5.7×10^{-2} $M_{\oplus}$, or 4.9 $M_{\rm Moon}$, or 0.5 $M_{\rm Mars}$ (Table 3). This mass of 3.4×10^{23} kg is similar to the amount of mass thought to have been present in the nascent solar system asteroid belt (Chambers 2004). Assuming that the emitting dust is derived from collisional grinding in a young, dense asteroid belt (scenario 4), we can use another method of mass estimation to give a similar result. Comparing our best estimate of the 0.1–1000 μm HD 113766A dust mass to the dust mass estimated to be in the solar system zodiacal cloud today (consisting mainly of 0.1–1000 μm dust particles), we find the HD 113766A dust to be $\sim 10^5$ times as massive. Assuming that the collisionally produced dust production rate goes as the total planetesimal belt mass squared, estimating half of the solar system zodiacal cloud to be asteroidal in origin, and ignoring small factors on the order of unity, we derive a mass for the warm HD 113766A dust, including all bodies, of $(10^5)^{1/2} M_{\rm asteroid\ belt} = 0.15 M_{\oplus} = 1.5 M_{\rm Mars}$. This is consistent with the 10 m maximum size estimate derived above, suggesting that there is probably much more dust mass present than definitively detected by the 5–35 μm *Spitzer* measurements. We thus include the 3.4×10^{23} kg estimate in the conservative range of HD 113766 total dust masses listed in Table 3. (Note that if we assume the presence of 1 km radius objects found in most current models of planet formation, we find a total dust mass of 0.5 $M_{\oplus}$, but we cannot support this upper size limit except by conjecture, and so do not quote it as a firm result, pending further work.)

The dust surface area is $\sim a^{-0.51}$ and is dominated by the smallest particles. From direct integration of the best-fit model PSD, we find a total estimated 0.1–20 μm surface area from the IRS data of 1.2×10^{22} m^2, or 0.54 AU^2. Assuming that the dust is in a ring centered at 1.8 AU from the central star, in an annulus 0.4 AU wide (± 2 σ in the best-fit model radius) and with total surface area 1.1×10^{23} m^2, we find a spatial filling factor of 0.11 for the dust. It is interesting to note that the fraction of the illuminated sphere at 1.8 AU covered by dust is $1.2/(4\pi^* 1.8^2) = 0.029$, close to the $L_{\rm IR}/L_* = 0.015$ value (Chen et al. 2006). Allowing for energy losses due to scattering (i.e., an average Bond albedo for the dust of 10%–20%, as found for micron-sized dust emitted from solar system comets [Lisse et al. 2002]) improves the agreement even further. We can also say something about the opening angle of the disk: the inclinations of disk particles must be greater than 3.7° (0.064 rad) for the dust to intercept enough of the HD 113766A luminosity to explain the IR luminosity. Even at inclinations of $\sim 4°$, the disk would have to be optically thick along the midplane. An optically thick disk also implies that the total disk mass estimate of 3.4×10^{20} kg presented above is a

conservative lower limit for the actual total disk mass. The same arguments apply in the case of a 10 m largest particle.

5. DISCUSSION: NATURE OF THE HD 113766 DUST

In § 1 we presented five possible physical scenarios for the source of the warm dust in HD 113766: (1) primordial material, (2) ongoing evaporation of material from a large swarm of primitive icy planetesimals (comets), (3) collisions of many bodies within a massive comet or asteroid (processed, differentiated planetesimals) belt, (4) a recent collision between two large comets or asteroids in a planetesimal belt, or (5) a recent collision between two protoplanets. Here we utilize the results of the modeling presented in § 4 to eliminate all incompatible scenarios, then discuss what the source(s) of the dust must be.

5.1. *Noncometary Composition*

The circumstellar material around HD 113766 does not appear to be primitive, i.e., derived from a cometary source containing abundant water and carbon-bearing species (PAHs, CO_2, carbonates, organic ices, etc.), like the circumstellar material around the HD 100546 system or in comets T1 and Hale-Bopp (Lisse et al. 2006, 2007a). We can verify this hypothesis by directly comparing the HD 113766 and HD 100546 disk spectra (Fig. 2), noting the absence of features in the 5–9 μm region due to PAHs, amorphous carbon, water gas, and carbonate species in HD 113766. The HD 113766 material appears instead to be compositionally close to that of igneous rocks on the Earth, lacking in all but the most refractory amorphous carbonaceous component (akin to terrestrial soot or volcanic ash).

We also see evidence for processing of the HD 113766A dust in the compositional olivine/pyroxene trend plot of Figure 7, created by analyzing the *ISO* and *Spitzer* mid-IR spectra of nine dusty systems using our compositional model (Lisse et al. 2007c), along with a ground-truth point calculated utilizing the latest bulk ratios for the *Stardust* comet Wild 2 sample return (Zolensky et al. 2007). As the extremes of the trend plot are found in the dust around YSOs and in the elderly white dwarf systems, the overall trend is for the pyroxene content of a system to decrease with increasing system age and material processing. We attribute the apparent trend to the fact that pyroxene materials are less refractory and thermodynamically stable than olivine materials and, thus, less resistant to high temperature and pressure changes inflicted on system material due to collisions, gravitational accretion, differentiation, radioactive decay, and stellar heating on megayear to gigayear timescales. The relative effect of each of these processes depends not only on the age of the dust but also on its location with respect to the system primary and the parent-body history of the dust. For example, compare the SW1 location to that of the four solar system comets T1, Hale-Bopp, SW3, and Wild 2 in the silicate trend plot of Figure 7. SW1, while also a relatively primitive, icy outer solar system body, is large enough to have undergone significant alteration due to Al^{26} radiogenic heating and solar insolation during its formation (Merk & Prialnik 2006; Toth & Lisse 2006), while retaining a solar atomic abundance (as determined from our compositional modeling).

On the olivine/pyroxene trend line, we find that HD 113766 appears to be more similar to the asteroidal debris disk material found around HD 69830 (Beichman et al. 2005; Lisse et al. 2007b) and, by direct comparison, to asteroidal material in the HD 69830 system. It also lies in a location similar to that of the material emitted from the large, differentiated, refractory solar abundance Centaur body SW1. We conclude from the mineralogical evidence that the HD 113766A circumstellar material is derived from a processed and differentiated parent asteroidal/protoplanetary body or bodies, and we can rule out the following primitive cometary body scenarios as the source of the warm dust in HD 113766: (1) residual primordial material, (2) sublimation from comets, (3) collisional fragmentation of comets in a dense belt, or (4) the disruption of a supercomet planetesimal. We are left to consider scenarios 3 and 4 for asteroids or protoplanets or scenario 5 for the spallation of surface material from a protoplanet during a lunar formation event.

5.2. *Dust Parent Body*

Our derived mineralogy suggests the likely progenitor(s) were similar in composition to an S-type asteroid (in the Tholen taxonomy; e.g., Lodders & Fegley 1998, Table 13.7, p. 250, and references therein), bodies commonly thought to be the source of much of the terrestrial planets' mass. As discussed in § 1, at 10–20 Myr in our solar system, the giant planets hade already formed, nebular gas had mostly cleared, and the terrestrial planets had begun to coalesce. It is thus very reasonable for us to observe the effects of dusty aggregation of rocky terrestrial planet material in the *Spitzer* spectra of HD 113766. These effects could be causing dust either by collisional grinding between asteroids in a dense belt as small rocky planetesimals slowly aggregate into larger bodies (scenario 3), or by catastrophic collisions between two large asteroidal bodies of the size of planetary embryos or oligarchs ($\sim M_{\rm Ceres}$; scenario 4).

The near-solar atomic abundance of the refractory species in the best-fit spectral model cannot distinguish between these two scenarios. Solar-abundance dust can be evidence for production from a large collection of differentiated objects, averaging out to solar values, or for the youth and primitive nature of the parent body (or bodies), reflecting the original mix of solar abundance materials from which they formed. We thus made an attempt to learn more about the putative parent bodies of the dust observed in the HD 11376 system using the mineralogical, as well as the atomic, information derived from the *Spitzer* spectra, by comparing the best-fit spectral model results for the classes of material present to compositional measurements of solar system meteorites. Following Stoeckelmann & Reimold (1989), a mixing calculation was performed using modal data (normalized by volume or percent by volume) of the mineralogical composition of meteorites from the literature (Jarosewich 1990; Papike 1998; Hutchison 2004; Warren et al. 2006). We note that our calculations are highly simplified; only the mineral components occurring in the HD 113766A spectrum were used for the calculations. All crystalline olivines were added and used as the total amount of olivine for the calculations (same with pyroxene-class minerals). All the various sulfide mineral components were grouped together, as were the phyllosilicates. All carbon (graphite) was counted as amorphous carbon. For carbonaceous chondrites, the carbon contained in volatile species was assumed to be destroyed by any collisional mechanisms and was ignored. For the iron meteorites, a simplified "model iron meteorite" with only carbon, iron, and sulfide was used.

Allowing for the simplicity of our modeling, the fact that modal data for all meteorite types is not available, and the fact that meteoritic materials show a very wide range in composition, we nevertheless find that three of the mineral class results from HD 113766A are highly diagnostic and allow us to limit the number of potential meteoritic components:

Metal sulfides.—Most meteorites rarely have more than 10% by volume of sulfides (stony enstatite chondrites can get up to about 16% by volume). To get to 25% by volume of HD 113766A, only iron meteorites (highly differentiated meteorites consisting

of nickel-iron metal and sulfides and related siderophile species) are possible. Iron meteorites can contain up to about 50% sulfides by volume.

Amorphous carbon.—Most meteorites contain hardly any carbon. Exceptions are the iron meteorites, ureilites (relatively primitive achondrites, or stony meteorites), and carbonaceous chondrites (CCs; very primitive meteorites of near-solar abundance). However, in most of the CCs the carbon is in organic material, for which no evidence is seen in the IRS spectra (and which probably would not survive collisional processing). Ureilites contain about 14% carbon by volume, mostly graphitic. In iron meteorites, clasts of graphite are also common in abundances similar to that in HD 113766A.

Phyllosilicates.—Phyllosilicates as alteration products usually occur in the primitive CC meteorites like Murchison CM2, Orgueil CI1, or Tagish Lake C2.

For HD 113766, these constraints imply that all allowable meteorite fits ($\chi^2 < 1$) show a mixture of stony meteorite (achondrite, specifically ureilite) at 37%–59% by volume, sulfide-rich iron meteorite at 27%–33% by volume, and primitive CC between 7.9% and 8.3% by volume. Stony meteorites dominate the mix; the best fits were found for a mixture of 37% ureilite, 27% iron, 8% Murchison, and 27% ordinary LL3.4 chondrite (another stony meteorite). However, as long as the three species (ureilite, iron, and CC) were in the mixture, one could add a mix of most other stony meteorite types (at 20%–30% by volume) and still get a good fit. This finding is consistent with an S-type asteroid as the parent body for the observed dust.

How can we interpret these results? The linkage between specific types and classes of meteorites and the asteroids is sometimes difficult. There are problems in observing the mineralogical composition of an asteroid surface at a quality good enough to distinguish different types of meteorites, as well as in allowing for the effects of space weathering on the spectral properties of asteroid surface material. Classification is based on a few spectral characteristics (optical/near-IR) and mineral ratios, which can indicate various groups of meteorites. It is also important to take into account that no meteorite represents the composition of a whole asteroid and that meteorite sample we have, and sample biases are large. For example, current models predict that multiple large protoplanetary bodies, long since collisionally disrupted or dynamically removed, were formed from the protoplanetary disk in the early asteroid belt, and upward of 99% of the original mass has been removed in forming the present-day asteroid belt. In the protoplanetary disk, Fe and S are of similar atomic abundance to Si and Mg, and the Fe has to be placed in some major reservoir as aggregation occurs. So, for any stony material linked to an achondrite or S-type asteroid, it is reasonable to expect in a primitive, unevolved circumstellar disk that there should also be material similar to what is found in iron meteoritic material contained in metal/metal sulfide–rich inclusions, hidden cores, or metallic asteroids (e.g., M types; Burbine et al. 2002). Yet metallic asteroids and meteorites are relatively rare in the solar system.

Given these caveats, complete disruption of a mildly processed, semidifferentiated, ureilite-dominated stony parent body with metallic/metal-sulfide inclusions and/or core is the best candidate we find for producing the HD 113766A circumstellar disk material. Ureilites are common primitive achondrites (stony meteorites), the second most abundant after the HED group. The ureilite parent body (S-type) is thought to be >100 km in radius (Warren et al. 2006), on roughly the same size scale as the body we estimate to have produced the HD 113766A dust. CCs, the most common and most primitive of the meteorites formed from the protoplanetary disk, are the likely starting material for ureilites (Warren et al. 2006; Goodrich et al. 2007). The melt produced by heating up CCs to get ureilites is metal sulfide–rich, providing the material for the iron meteoritic component we find in our meteorite model. The CC material required by the meteorite fit could be interpreted as a nonaltered leftover from the precursor material used to form the ureilite-dominated stony parent body. Alternatively, the CC material found in our meteoritic fit could have been part of a second, primitive body involved in the two-body collision that created the observed dust. Either physical picture is consistent with the location of HD 113766 in the olivine/pyroxene silicate trend line (Fig. 7); CC-urelite the dusty material is more processed than the stuff composing comets but is less reworked and differentiated than material found in mature asteroids. Either case supports an asteroidal parent-body fragmentation scenario (4) as the source of the observed dust.

It is important to note that we have not allowed here for collisional shock effects on the initial parent mineralogy in scenario 4. While the overall effect of shocks in large-body collisions is relatively unexplored and uncertain, and further work needs to be done in this area, we can get an estimate of these effects using the studies on shocked Murchison samples (Tomioka et al. 2007). Their major finding was the production of abundant amorphous silicate phases of a similar nature to that of the amorphous silicates used in our spectral modeling. Since these phases are relatively rare in ureilites, iron meteorites, and CCs, in the impact scenario between two bodies of these types the amorphous materials could be impact products and evidence for impact-produced processes. We also note that there is no reason that the dust has to be created in just one large two-body collision—as in scenario 3, collisional grinding dust production in a dense asteroid belt—but we reserve judgment on the results of the meteorite modeling concerning this scenario, as the lack of compositional data for all meteorite types at the time of this writing negates our ability to build an entire asteroid belt and average over the expected collision products.

Another possibility is that we are witnessing scenario 5, thermal emission from dust created by a massive collision and partial spallation event between two large, highly differentiated protoplanetary bodies, such as is thought to have formed the Earth's Moon (Benz et al. 1986; Canup 2004 and references therein). Similar arguments were put forth by Telesco et al. (2005), who found a large excess "clump" of emission (at ~50 AU) in mid-IR thermal images of the similarly aged β Pic system (~12 Myr) and determined that small dust grains making up the clump most likely originate from a recent planetesimal collision during the latter stages of outer icy planet formation in that system. However, the material spun off the accreting Earth by the impact of an approximately Mars-sized body was rich in light Mg-rich silicates and Al oxides (outer crustal material) and poor in Fe and other heavier refractories, unlike the near-solar atomic refractory abundances and the large molar fraction of metal sulfides we find for the HD 113766 circumstellar material (§ 4.1). We can thus rule out a lunar-formation-type scenario (5) for creating the observed circumstellar material and focus instead on the interactions of bodies smaller than the Moon and more primitive (less differentiated).

5.3. *Dust Location versus the Primary*

The location of the warm dust excess is in the inner system region, exactly where terrestrial planet formation is expected to occur. The net temperature of the dust is such that the majority of icy materials should be in gaseous form. Little evidence for gas emission has been found in the system, however, allowing us to conclude that the dust-to-gas ratio of the ~440 K circumstellar

material is very high, favoring rocky planet formation and scenario 3 or 4 for processed planetesimals (asteroids) as the source of the HD 113766A dust. The 1.8 AU distance of the dust belt from the primary is equivalent to a distance of 0.9 AU in the solar system. The potential of material located so close to HD 113766A to form a terrestrial planet is not significantly affected by HD 113766B at 170 AU average distance (Quintana et al. 2007). The location of water in the form of icy dust at 4–9 AU, apparently straddling the system's snow line, is also quite reasonable and has an analog in current models of early solar system formation (Kuchner 2003; Raymond et al. 2004).

5.4. *Dust Mass*

The mass of the observed warm dust, $\geq 3 \times 10^{20}$ kg, and its equivalent single asteroidal body (density = 2.5 g cm^{-3}) size, $\geq$320 km (radius), is the size of the bodies believed to be critical to the formation of Earth-like planets in the latter part of their growth period. If, instead, the 3×10^{20} kg consisted of cometary material, it would represent the mass of about 1 million average solar system comets (Table 3). However, if derived from a million comet-like objects, there would be a concomitant large amount of gas in the system, including water gas, as typical solar system comet ratios of emitted gas-to-dust mass lie in the range 0.3–3.0 (Lisse et al. 2002). We know the HD 113766 system is gas-poor, by about a factor of 4, versus the ISM gas-to-dust ratio of $\sim$100 from the observations of neutral hydrogen lines by Chen et al. (2006). While the neutral hydrogen result tells us that much of the protostellar nebular gas has been removed and giant planet formation has finished, it is not very restrictive on the presence of comets in the system. A stronger limit is found by the nondetection of water gas emission in the spectrum analyzed in this work. Using a conservative upper limit, at the 95% CL of 0.01 relative surface area (Table 1), we find roughly one-seventh as much water gas to dust as was seen in the comet T1 ejecta (Lisse et al. 2006). The ejecta was shown to have a gas-to-dust ratio of $<$0.77, so the HD 113766 gas-to-dust ratio is $<$0.1, very low for a cometary system, again disfavoring a source for the dust from cometary emission (scenario 2).

We can rule out the other possible icy parent-body scenario as well. If instead the observed material had been aggregated into a single cometary parent body (scenario 4) before its release in a catastrophic breakup, 10^{20} kg of material would have densified and differentiated (Toth & Lisse 2006; Jewitt et al. 2007). This processing would transform the original cometary material into substances more typical of the outer icy moons and dwarf icy planets—high-density ice phases, large particles of conglomerate rock, and aqueous alteration products like carbonates, sulfates, and phyllosilicates—which we do not find dominating the warm dust spectra. On the other hand, this mechanism could have led to the production of the icy dust we see located at $\sim$9 and 30–80 AU from HD 113766A. (Unfortunately, because of the low temperatures for the icy dust, the short-wavelength diagnostic features in the IRS passband are highly attenuated. Since we have so little information on the amount and kind of cold dust in these reservoirs, we do not examine them further, but note that future spectral observations with higher spatial resolution may very well produce important new findings on the cold dust.)

5.5. *Aged Dust?*

Could the system be a very slowly aging or slightly modified primordial disk, as predicted by scenario 1? Probably not. The free gas-to-dust ratio we find for the circumstellar material is on the order of 1000 times lower than the ISM values. Using the $\sim$10 Myr old HD 100546 as an example of a primordial dusty disk system, we note that the HD 113766 PSD is much more heavily weighted to larger particles. Whether this is due to evolution of the HD 113766 dust due to aggregation and agglomeration creating larger dust or to radiation pressure and P-R drag preferentially removing the smallest dust is not clear. Dynamical effects are certainly important for the 10–16 Myr old HD 113766 system—for the smallest dust detected, 0.1 μm, the ratio of the radiation force to stellar gravity, β, is approximately 1.0, and such dust is removed from the system by radiation pressure on orbital timescales as soon as it is created. For the largest warm dust we consider, 20 μm and $\beta \sim 0.03$, it would take 10^4–10^5 yr for this dust to spiral in by P-R drag (Burns et al. 1979), where it would evaporate. As noted in § 5.1, the mineralogy of the warm HD 113766 dust is very different from the primitive, comet-like material found around HD 100546, being much more processed and evolved. Finally, we note that the amount of dust mass is about a factor of 30 lower than the lower mass limit for HD 100546 from *ISO* (Table 3), indicating that the large majority of the HD 113766 disk has been sequestered or removed.

In sum, the HD 113766 warm circumstellar material appears to be in a fundamentally nonprimordial regime, one much more likely to be derived from collisions in a massive asteroid belt (scenario 3) or from disruption of a large processed parent body (scenario 4; cf. the HD 69830 system; Beichman et al. 2005; Lisse et al. 2007b) than to be derived from a primordial nebula dominated by primitive cometary material, like HD 100546. Despite the reported lack of strong spectral features on whole-system scales (Pantin et al. 1999; Chen et al. 2007), the $\sim$12 Myr old A5 β Pic system may be a closer behavioral analog, as suggested by recent high spatial resolution studies using the Subaru telescope providing evidence for three narrow circumstellar belts of enhanced small silicate particles (Okamoto et al. 2004).

5.6. *Future Work*

Future measurements of this system will be highly valuable in further elucidating the mechanisms currently in play. The two most likely source mechanisms for the dust given here (scenarios 3 and 4) should have different temporal signatures. The ongoing collisional grinding of an extremely dense young asteroid belt undergoing collisional aggregation should yield roughly constant spectral behavior with time, perhaps with stochastic increases when fresh collisions occur, while the breakup of a large, >320 km radius, S-type body should demonstrate a monotonically decaying dust spectral signature and density with time. The relative constancy of the mid-IR excess emission detected for this system (Fig. 1) over the 20 yr time between the *IRAS* and *Spitzer* observations would seem to argue against any single impulsive events and for continual collision processes, although we caution that 20 yr may not have been long enough for the dust-clearing mechanisms to operate fully and allow us to distinguish between the two possibilities.

Observations of the system at submillimeter, millimeter, and radio wavelengths (*Herschel*, ALMA) will also be highly useful, allowing us to put better lower limits on the total mass of dust and ice in the system. Spatial studies of HD 113766 might be able to distinguish between the different mechanisms by searching for "clumps," or localized condensations of dust formed in a single breakup or collision, versus the smooth distribution expected from collisional grinding throughout a thick asteroid belt. However, to achieve this will require resolution at the $(2\ \mathrm{AU}/120\ \mathrm{pc})(1''/1\ \mathrm{AU}) = 16$ mas level, making direct imaging of the warm dust torus problematic even with the multimeter-aperture *James Webb Space Telescope*, although useful upper limits to the radial extent of the dust will most likely be obtained.

6. CONCLUSIONS

1. We have obtained excellent fits to the 5–35 μm mid-IR spectra of the dusty disk system HD 113766 using the *Deep Impact* T1 ejecta model.

2. Only olivines, pyroxenes, Fe-rich sulfides, amorphous carbon (or native Fe:Ni), and water ice are found in abundance in the disk material of the system. Apart from the water ice, the mix of materials is close to that found for common S-type asteroids in our solar system.

3. Assuming the central star to have a luminosity $L_* = 4.4\,L_\odot$, we locate the refractory material causing the observed emission at 1.8 ± 0.2 (2 σ) AU. If this material had formed in our solar system, it would have been located at 0.9 ± 0.1 (2 σ) AU. The majority of the detected water ice may be colocated or as far out as 9 AU from HD 113766. There is also evidence for another zone of cold dust at 30–80 AU from the system primary.

4. The amount of mass in 0.1–20 μm particles responsible for the observed IR emission excess is at least 3×10^{20} kg, equivalent to an asteroidal body of 320 km radius (assuming 2.5 g cm^{-3} density). Extrapolating up to a 10 m largest particle, we estimate the amount of mass present to be at least 3×10^{20} kg, or $0.5\,M_{\rm Mars}$. Assuming 1 km planetesimals are present, the warm dust mass is $\geq 0.5\,M_\oplus$.

5. Despite a similarity in ages, the 10–16 Myr old F3 HD 113766A system is clearly not an older analog of the primitive, giant-planet-forming, >10 Myr old HD 100546 A0e V system, which is dominated by cometary material and has an extensive, massive primordial disk (Lisse et al. 2007a). The ~12 Myr old A5 β Pic system is a closer analog for solar system formation.

6. We find the source for the observed excess emission to be either the complete disruption of an approximately S-type, $\geq$320 km radius (terrestrial-planet-forming) body or a very dense asteroid belt made up of a large number of small S-type bodies undergoing continual aggregational collisions. Either of these possibilities is a predicted outcome of terrestrial-planet formation processes, making this system an exciting and potentially groundbreaking object for future study.

Note added in manuscript.—New work by I. Song et al. (2007, private communication) quotes an age for the Lower Centaurus Crux association and thus the HD 113766 system of 10 Myr.

This paper is based on observations taken with the NASA *Spitzer Space Telescope*, operated by JPL/CalTech. C. M. L. gratefully acknowledges support for performing the modeling described herein from JPL contract 1274485 and the APL Janney Fellowship program. The authors would also like to thank M. Meyer for many valuable discussions and comments in improving this work.

REFERENCES

A'Hearn, M. F., et al. 2005, Science, 310, 258
Augereau, J. C., et al. 2001, A&A, 370, 447
Backman, D. E., & Paresce, F. 1993, in Protostars and Planets III, ed. E. Levy & J. I. Lunine (Tucson: Univ. Arizona Press), 1253
Beichman, C. A., et al. 2005, ApJ, 626, 1061
———. 2006, ApJ, 639, 1166
Benz, W., et al. 1986, Icarus, 66, 515
Bottke, W. F., et al. 2005, Icarus, 175, 111
Bryden, G., et al. 2006, ApJ, 636, 1098
Burbine, T. H., McCoy, T. J., Meibom, A., Gladman, B., & Keil, K. 2002, in Asteroids III, ed. W. F. Bottke, Jr., et al. (Tucson: Univ. Arizona Press), 653
Burns, J. A., Lamy, P. L., & Soter, S. 1979, Icarus, 40, 1
Canup, R. 2004, Icarus, 168, 433
Cardelli, J. A., Clayton, G. C., & Mathis, J. S. 1989, ApJ, 345, 245
Chambers, J. E. 2004, Earth Planet. Sci. Lett., 223, 241
Chen, C. H., et al. 2005, ApJ, 623, 493
———. 2006, ApJS, 166, 351
———. 2007, ApJ, 666, 466
Currie, T., et al. 2007a, ApJ, 659, 599
———. 2007b, ApJ, 663, L105
Cutri, R. M., et al. 2003, 2MASS All-Sky Catalog of Point Sources (Pasadena: IPAC/Caltech)
de Zeeuw, P. T., et al. 1999, AJ, 117, 354
Dohnanyi, J. W. 1969, J. Geophys. Res., 74, 2531
Draine, B. T., & Li, A. 2007, ApJ, 657, 810
Durda, D. D., & Dermott, S. F. 1997, Icarus, 130, 140
Furlan, E., et al. 2007, ApJ, 664, 1176
Goodrich, C. A., Van Orman, J. A., & Wilsom, L. 2007, Geochim. Cosmochim. Acta, 71, 2876
Grogan, K., et al. 2001, Icarus, 152, 251
Harker, D. E., et al. 2005, Science, 310, 278
Higdon, S. J. U., et al. 2004, PASP, 116, 975
Hines, D., et al. 2006, ApJ, 638, 1070
Hutchison, R. 2004, Meteorites: A Petrologic, Chemical and Isotopic Synthesis (Cambridge: Cambridge Univ. Press)
Jarosewich, E. 1990, Meteoritics, 25, 323
Jewitt, D. C., et al. 2007, in Protostars and Planets V, ed. B. Reipurth, D. Jewitt, & K. Keil (Tucson: Univ. Arizona Press), 863
Jura, M. 2006, ApJ, 653, 613
Kalas, P., Graham, J. R., & Clampin, M. C. 2005, Nature, 435, 1067
Kalas, P., Graham, J. R., Clampin, M. C., & Fitzgerald, M. P. 2006, ApJ, 637, L57
Keller, H. U., et al. 2005, Science, 310, 281
Kenyon, S. J., & Bromley, B. C. 2004a, AJ, 127, 513
———. 2004b, ApJ, 602, L133
———. 2006, AJ, 131, 1837
Kuchner, M. J. 2003, ApJ, 596, L105
Lien, D. J. 1990, ApJ, 355, 680
Lisse, C. M., A'Hearn, M. F., Fernandez, Y. R., & Peschke, S. B. 2002, in Proc. IAU Colloq. 181, Dust in the Solar System and Other Planetary Systems, ed. S. F. Green et al. (Amsterdam: Pergamon), 259
Lisse, C. M., et al. 1998, ApJ, 496, 971
———. 2006, Science, 313, 635
———. 2007a, Icarus, 187, 69
———. 2007b, ApJ, 658, 584
———. 2007c, LPI Contrib., 1338, 2259
Lodders, K. 2003, ApJ, 591, 1220
Lodders, K., & Fegley, B. 1998, The Planetary Scientist's Companion (New York: Oxford Univ. Press)
Malfait, K., et al. 1998, A&A, 332, L25
Mamajek, E. E., Lawson, W. A., & Feigelson, E. D. 1999, ApJ, 516, L77
Mamajek, E. E., Meyer, M. R., & Liebert, J. 2002, AJ, 124, 1670
Matthews, B. C., Kalas, P. G., & Wyatt, M. C. 2007, ApJ, 663, 1103
Merk, R., & Prialnik, D. 2006, Icarus, 183, 283
Meyer, M. R., et al. 2001, BAAS, 33, 1420
Nesvorny, D., et al. 2003, ApJ, 591, 486
———. 2006, Icarus, 181, 107
Nordstrom, B., et al. 2004, A&A, 418, 989
O'Brien, D. P., & Greenberg, R. 2003, Icarus, 164, 334
Okamoto, Y. K., et al. 2004, Nature, 431, 660
Pantin, E., Waelkens, C., & Malfait, K. 1999, in The Universe as Seen by *ISO*, ed. P. Cox & M. F. Kessler (ESA-SP 427; Noordwijk: ESA), 385
Papike, J. J. 1998, Planetary Materials (Washington: Mineral. Soc. Am.)
Quintana, E., et al. 2007, ApJ, 660, 807
Raymond, S. N., Quinn, T., & Lunine, J. I. 2004, Icarus, 168, 1
Reach, W. T., et al. 2005, ApJ, 635, L161
Rhee, J. H., Song, I., & Zuckerman, B. 2007, ApJ, 671, 616
Ronov, A. B., & Yaroshevsky, A. A. 1969, in The Earth's Crust and Upper Mantle, ed. P. J. Hart (Washington: Am. Geophys. Union), 37
Sadakane, K., & Nishida, M. 1986, PASP, 98, 685
Schleicher, D., et al. 2006, AJ, 131, 1130
Schutz, O., Meeus, G., & Sterzik, M. F. 2005, A&A, 431, 175
Stansberry, J. A., et al. 2004, ApJS, 154, 463
Stoeckelmann, D., & Reimold, W. U. 1989, Math. Geol., 21, 853
Sugita, S., et al. 2005, Science, 310, 274
Sunshine, J. S., et al. 2006, Science, 311, 1453
Sylvester, R. J., et al. 1996, MNRAS, 279, 915

Telesco, C. M., et al. 2005, Nature, 433, 133
Thebault, P., Augereau, J. C., & Beust, H. 2003, A&A, 408, 775
Tomioka, N., et al. 2007, Meteoritics Planet. Sci., 42, 19
Toth, I., & Lisse, C. M. 2006, Icarus, 181, 162
Walker, H. J., & Wolstencroft, R. D. 1988, PASP, 100, 1509
Warren, P. H., et al. 2006, Geochim. Cosmochim. Acta, 70, 2104
Watson, D., et al. 2004, ApJS, 154, 391
Wetherill, G. W. 1990, Annu. Rev. Earth Planet. Sci., 18, 205
Williams, D. R., & Wetherill, G. W. 1994, Icarus, 107, 117
Wooden, D. H., et al. 1999, ApJ, 517, 1034
Wyatt, M. C., & Dent, W. R. F. 2002, MNRAS, 334, 589
Wyatt, M. C., et al. 2007, ApJ, 658, 569
Yin, Q., et al. 2002, Nature, 418, 949
Zolensky, M., et al. 2007, LPI Contrib., 1338, 1481
Zuckerman, B., & Song, I. 2004, ARA&A, 42, 685
Zuckerman, B., et al. 2001, ApJ, 562, L87